Experimental analysis of 3D cracking in drying soils using Ground Penetrating Radar

Héctor U. Levatti[1], Pere C. Prat[2], Alberto Ledesma, Agustín Cuadrado & Josbel A. Cordero

Dept. of Civil and Environmental Engineering, UPC-BarcelonaTECH, Spain

ABSTRACT

This paper describes the capabilities of a novel technique to investigate crack formation and propagation in drying soils. The technique is a relatively simple, non-destructive indirect technique using a ground penetrating radar (GPR) system to detect cracks that form and propagate inside a soil specimen during desiccation. Although GPR devices have been used for multiple applications, their use in soils for the detection of small desiccation cracks has not been demonstrated yet. The experiment and the methodology used to test the accuracy of a small compact commercial GPR device for crack identification are described. The main objective was to identify what type of signals and what crack width and separation between them can be detected using the GPR device. The results indicate that cracks of one or two millimetres wide can be detected depending on its position and shape while sub-millimetre cracks are undetectable with the currently existing devices in the market. Regardless of this limitation, the GPR method can be useful to find time-related bounds of when the cracks appear, to point at their location and sometimes at the separation between two of them. Detection of cracks with origin at the bottom or within the specimen was accomplished with this system. Distances of 5 cm or more between cracks can be detected and measured as well with accuracy.

KEY WORDS: desiccation cracks, auscultation, ground penetrating radar

[1] Present affiliation: College of Engineering, Swansea University, Bay Campus, SA1 8EN, Swansea, UK.

[2] Corresponding author — Dept. of Civil and Environmental Engineering, UPC-BarcelonaTECH;
Jordi Girona 1-3, Building D2; 08034 Barcelona, Spain. Phone: +34 934016511; e-mail: pere.prat@upc.edu

Introduction

Soils made of clay or silt tend to shrink and crack when subjected to desiccation. The drying process is very complex in soils and includes physical, chemical, hydraulic and mechanical phenomena. The crack patterns are unique and its development depends on many factors. From the experimental point of view, several authors have studied this process since the early twentieth century (Haines 1923; Jahn 1950; Knechtel 1952; Lachenbruch 1961; Lambe 1958; Longwell 1928; Simpson 1936; Skempton and Northey 1952; White 1961; Willden and Mabey 1961) and many significant contributions have been made in the last half century (Ávila 2004; Chertkov 2002; Corte and Higashi 1960; Hu et al. 2008; Kodikara et al. 2000; Kodikara et al. 2004; Lakshmikantha 2009; Lakshmikantha et al. 2009, 2012; Lakshmikantha et al. 2013b; Lau 1987; Morris et al. 1992; Nahlawi and Kodikara 2006; Péron et al. 2009; Rodríguez et al. 2007; Tang et al. 2011; Vogel et al. 2005). However, until the development of unsaturated soil mechanics the problem has not been analysed considering the parameters that govern the behaviour of soil in the unsaturated state, primarily suction. Tensile strength (suction dependent) and fracture toughness are shown as the most relevant parameters (Ávila 2004; Lakshmikantha et al. 2012), but a definite model explaining that process is yet to be formulated.

In laboratory tests many cracks appear on the top boundary of soil specimens. However, there are others that are not visible and several experiments have shown that cracks may start at any point within the specimen (Lakshmikantha et al. 2009; Lakshmikantha et al. 2013a, 2016; Levatti 2015). To detect the cracks that start at the bottom boundary or within the sample one would need sophisticated techniques such as X-ray, magnetic resonance or electrical resistivity tomography (Hassan and Toll 2013; Mukunoki et al. 2010; Otani and Obara 2004; Samoulian et al. 2003), usually very expensive and involving very complicated setups. However, detection of those non-visible cracks is important because cracking due to drying in soils

is a very complex three-dimensional process and the study cannot limit itself to the outer visible cracks.

This paper presents a relatively simple, non-destructive, indirect technique using a Ground Penetrating Radar (GPR) device to detect cracks that form and propagate within the specimen during desiccation (Cordero et al. 2014; Levatti 2015; Prat et al. 2013). While continuous monitoring of surface cracking allows following the evolution of the external cracking pattern with time, the GPR technique may be helpful to detect the cracks within the soil, giving a more complete picture of the phenomenon with greater accuracy.

The main objective of this work is to identify what type of signals, and what crack width and separation can be detected using a small commercial GPR device. The ability to detect cracks which initiate at the bottom or inside the soil mass and appear later on the top of the specimen needed also to be demonstrated. The results indicate that cracks of one or two millimetres wide can be detected depending on its position and shape. Separations of 5 cm or more are easily detected and can be measured with accuracy. On the other hand, sub-millimetre cracks are undetectable with the currently existing devices in the market. The proposed method can also be useful to estimate when and where the cracks initiate with sufficient accuracy.

Basic Principles of a Ground Penetrating Radar System

The GPR is a non-destructive technique that uses electromagnetic pulses to detect reflecting surfaces inside the soil allowing imaging of buried objects, stratigraphy and other soil features at shallow depths, providing continuous, real-time profiles of the subsurface. The equipment consists of a computerized control system connected to antennas that are moved slowly along a predefined path on the ground surface to produce a continuous subsurface profile. One antenna emits the electromagnetic pulses and a second one records the reflected signals from the objects, discontinuities or other features inside the soil. The reflected wave originates from

changes in the electromagnetic properties of the soil that may be caused by variations in water content, density changes due to the presence of stratigraphic surfaces and discontinuities or voids existing in the path of the pulse. Therefore, the success of the technique relies, to a great extent, on a sufficient dielectric contrast at the crack location to produce a clear reflected signal. The penetration depth of the pulses, and data resolution, depend on the wavelength and the soil's dielectric constant. These parameters are mainly controlled by the soil's moisture content. The depth and resolution are inversely proportional magnitudes: increasing the antenna's frequency a better resolution is obtained but the depth is smaller.

The theoretical background of the method is the theory of electromagnetic fields, described by Maxwell's equations (1), and the constitutive equations (2):

$$\nabla \mathbf{D} = \rho_f; \quad \nabla \mathbf{B} = \mathbf{0}; \quad \nabla \times \mathbf{E} = -\frac{\partial \mathbf{B}}{\partial t} + \mathbf{M}; \quad \nabla \times \mathbf{H} = -\frac{\partial \mathbf{D}}{\partial t} + \mathbf{J} \tag{1}$$

$$\mathbf{D} = \varepsilon \mathbf{E}; \quad \mathbf{H} = \frac{\mathbf{B}}{\mu}; \quad \mathbf{J} = \sigma \mathbf{E} \tag{2}$$

where **E** = electric field, **H** = magnetic field, **D** = electric displacement field, **B** = magnetic induction, **J** = free current density, **M** = magnetization field and ρ_f = free charge density. The parameters that appear in Eqs (2) describe the electromagnetic properties of the medium and are: ε (dielectric permittivity), μ (magnetic permeability) and σ (electric conductivity).

The principle of a GPR is based on the dielectric permittivity, ε in Eq (2), which represents the permittivity of an electromagnetic pulse through the medium, compared to the void permittivity. It is a constant that gives a measure of the polarizing ability of a material in the presence of an electric field. This parameter is defined as the ratio of the capacitance of parallel plate electrodes containing dielectric material to the capacitance in a vacuum. The value provides an indication of the static response of the material when in the presence of an external electric field, i.e. describes how an electric field affects and is affected by the material. It is a non-dimensional parameter that depends on the electric conductivity and the thickness of the

layer. For most of the components of the soil this parameter has a value between 1 (for air) and 80 (for water). The GPR produces results by detecting wave reflections produced while the wave crosses the boundary between two materials with different dielectric constant.

The magnetic permeability, μ in Eq (2) is associated with the magnetic induction of the magnetic field intensity. It measures the degree of magnetization that a material obtains in response to an applied magnetic field. The magnetic permeability of the soil's constituents is close to 1 (provided they are not ferromagnetic materials), independent of the frequency of the magnetic field. Therefore, this magnitude usually has no great influence and is assumed to be constant.

The electrical conductivity, σ in Eq (2), provides a measure of the response of the free charges existing in the material when in the presence of an external electric field. It is a material property that expresses the proportionality between the electric field applied and the electric current due to the movement of the free charges, and provides a measure of the ability of a material to conduct an electric current, according to Ohm's law in Eq (2).

The majority of soils and rocks that form the Earth's crust are composed of silicate minerals, which are electrical insulators (Morrison and Gasperikova 2015). Electrical currents in these materials can only be carried by ions within the fluids filling the pores between the minerals. In that case, the conductivity depends mainly on the water content and on the chemical composition of the salts dissolved in the pore water. On the other hand, some materials such as metallic ore minerals or graphite are electrical conductors or semiconductors in which the electric current is carried by electrons. Except in this latter case, for most rocks and soils where current is carried by ions in the pore fluid, the conductivity depends on the porosity, salt concentration in the pore fluid, temperature, degree of saturation, pressure and clay content. In general, the conductivity increases with water content, concentration of salts, porosity, and clay content.

Because electric currents (electromagnetic waves in general) propagate through the pore water in soils, it is important to discuss the behaviour of such electromagnetic waves in the water in which they propagate at very low speed and with high attenuation. Water has a high effective dielectric permittivity, and the large contrast with the dielectric permittivity of the other soil components significantly influence the average speed of propagation of the electromagnetic waves. Studies have shown that within normal frequencies in prospecting subsurface radar, the relative dielectric permittivity and electric conductivity of the medium increases with the degree of saturation (Knoll and Knight 1994).

The presence of fine-grained material such as clay in the soils plays an important role in increasing its electric conductivity and dielectric permittivity. Because of atomic substitution, the clay particles are not electrically neuter, but have a net negative charge, therefore attracting cations to its surface from the surrounding fluid solution. The electrically charged particle surface plus the surrounding zone of decreasing cation concentration (double layer) has a higher conductivity than the pore water, providing an additional path for electrical currents along the surface of the mineral particles which increases both conductivity and dielectric permittivity (Brandes 2005; Mitchell 1993).

The electromagnetic parameters of the soil are also strongly dependent on the porosity. For a dry soil, a higher percentage of pores reduces the value of both conductivity and dielectric permittivity. However, if the soil is wet the effect is not as clear, and if the soil is fully saturated then the effect is reversed.

Soils are mixtures of different types of materials, each with its own electromagnetic properties. The overall electromagnetic properties of the soil depend on the properties of each constituent and its percentage in the mixture. Several models in the literature (Pérez 2001) can be used to estimate the value of the electromagnetic properties of the soil as a function of its porosity, water content and composition (mineral type and percentage). Using these models, it

can be seen that for a single-component material and for a given porosity, the range of variation of the electromagnetic properties depends greatly on the degree of saturation, and that the range increases with increasing porosity. All this indicates that the porosity, and the fluid contained in the pores, greatly influences the fluctuations of the electromagnetic properties, in particular of the relative permittivity and the electrical conductivity of the material. The pore fluid, in particular, is the main component controlling the values of the overall electromagnetic properties of the material. Because the ground is formed by three distinct phases (water, gas and solid) during the drying process, and the changes in time of each phase modify the soil's electromagnetic properties, there is added difficulty to the interpretation of the results.

Table 1 shows the electromagnetic properties of air and water under different states. Table 2 shows the electromagnetic properties of some soil constituents. This table illustrates the high variability of the dielectric constant and electrical conductivity, which depends largely on the constituent characteristics.

Experimental Program

The soil used for the tests is a red clay that has been characterized and studied repeatedly in previous works (Barrera 2002; Lakshmikantha 2009; Lakshmikantha et al. 2006) so its geological and mineralogical composition and its hydro-mechanical behavior are well known (Barrera 2002).

To study cracking under drying conditions, it appears necessary to monitor the cracking events that occur within the soil mass, so that internal cracks can be detected before they appear on the surface and become visible. This problem is a purely three-dimensional process and it is very difficult to carry out tests that monitor those 3D cracks. For that, one could resort to techniques such as X-ray radiography, magnetic resonance imaging (MRI) or computed tomography (CT) scans. All these techniques involve very sophisticated equipment which is very

expensive and that requires tightly controlled installations and environments to avoid leakage of radiation and contamination to avoid posing a health hazard to equipment operators or visitors. This type of equipment is commonly found in health facilities and hospitals to where it would be complicated to take specimens in a regular basis or for long periods of time. Buying such equipment for the sole purpose of the tests object of this paper would be, of course, out of the question because of the cost.

The use of Ground Penetrating Radar proposed in this paper has a much lower cost, therefore making it possible to acquire dedicated equipment for the tests. The technique has gained acceptance in recent years for subsurface imaging in geotechnical engineering and other civil engineering areas such as in detecting reinforcement bars in concrete structures or non-visible pipes in the ground or embedded in structures.

The GPR system that has been used in this work consists of a compact device (GSSI® *StructureScan Mini,* Figure 1) that includes two antennas (emitting and receiving), data-logger, basic software for in situ post-processing and a control screen for setup and management. Three laser beams are located at the bottom of the device to allow following predetermined paths with sufficient precision (Figure 1).

Table 3 shows the main technical specification of the device. The objectives of the tests described in this paper were mainly two: to detect and characterize the 3D cracking pattern inside the soil mass, and to determine the system's capabilities and limitations regarding its ability to detect cracks which develop within the soil mass and that therefore are not visible. The first objective can be achieved by a thorough post-processing of the data collected by the device using suitable software with the methodology developed by the authors (Prat et al. 2013). The second objective requires comparing the results of the post-processing with the external, visible cracks that will allow for calibration of the device's capabilities.

The experimental program consisted of three series of tests: (a) some preliminary tests in which the purpose was to determine the minimum crack opening that the device can detect and the influence of the orientation of the crack plane; (b) drying tests in which the specimen was dried at constant environmental conditions with the purpose of detecting internal cracks and checking the system capabilities and limitations; and (c) cyclic tests in which the specimen was subjected to drying/wetting cycles to investigate the effect of cycles in the crack pattern and for which the GPR device was used at some points during the test.

Block Specimen Tests

The first type of tests was conducted on specimens made using a rectangular planter pot, of the type commonly found in garden stores. The specimen shape allowed the use of less amount of soil for the required specimen depth. The purpose was to determine the minimum crack opening that the GPR device can detect. Several artificial cracks were induced in the specimen using five strips of different thickness and material that were inserted into the soil (Figure 2a), three vertical (A, metal, 6 mm; B, metal, 4 mm; and C, metal, 2 mm) and two horizontal (D, metal, 2 mm; and E, wood, 5 mm). After the strips were inserted in the mould the slurry was poured and left to dry in an open-air environment (Figure 2b). After one month of drying some cracks had appeared on the surface (Figure 2c) and the consistency of the specimen was hard enough to perform the GPR scan. This was conducted, without removing the strips, in the direction parallel to the longest side of the specimen (from right to left in the figure).

Figure 2d shows the GPR profile obtained shortly after the surface cracks became visible and before the strips were removed. The figure has a rounded rectangular box on top showing two diffraction patterns shaped as hyperbolas that indicate the position of the two surface cracks. Below is a squared rectangular box showing the location of the vertical strips (A, B, C) with three consecutive hyperbolas located approximately at the same depth. In the same figure an ellipse indicates the position of strips D and E. It is not clear whether the corresponding

hyperbolas have been really detected by the GPR or they are actually an overlap effect of the tail of the hyperbolas corresponding to strips C, B and A. The lower horizontal line delimits approximately the depth of the specimen.

The results of this test indicate that 1 to 2 mm-wide cracks can be detected depending on the position and shape and on the moisture content of the specimen. Higher moisture content and more superficial cracks result in easier detection and interpretation of the received signal. Cracks less than 5 mm wide and at depths of 8 cm or more are difficult to distinguish from the signal's background noise. Hairline or sub-millimetre cracks cannot be identified with the current GPR technology.

Drying Tests

Tests were carried out in the laboratory using the GPR on a drying soil specimen contained within a cylindrical tray of 80 cm in diameter and 10 cm high. Clay, initially in a slurry state, was poured into the tray and left to dry in the laboratory-controlled environment (air relative humidity of approximately 60% and temperature 24^{o}C) during 36 days. The GPR device was used periodically to check for crack formation and propagation within the soil mass, and in order to calibrate the soil's electromagnetic properties. The use of the device requires a smooth, even surface on which it can slide. For that purpose, a one cm-thick poly(methyl methacrylate), or PMMA, circular plate was placed above the specimen.

A grid defining the line paths along which the device takes readings was affixed on top of the plate (see Figure 3). The grid was shaped as a 30 by 30 cm square defining two sets of 7 orthogonal traverses with a separation of 5 cm. Therefore, the soil portion of the specimen that was scanned by the GPR device was a square prism of dimensions 30 by 30 by 10 cm, located at the centre of the specimen. The nominal thickness of 10 cm, however, decreased during the drying process to 7 to 8 cm depending on the initial moisture content of the specimen. Figure 3 shows the initial stage of the soil inside the tray and the PMMA plate with the grid.

The GPR device allows for dielectric constant (k) values in the range of 4 to 12. The best results for the tests reported were obtained with a value of 12. The depth setting for scaling of the device is between 20 and 40 cm, the closest to the tests being 20 cm. Because the depth of the specimen was 10 cm, the results show an additional portion of 10 cm corresponding to the bottom boundaries of the testing equipment.

Figure 4 shows the evolution of the specimen subjected to desiccation during the 36 days that the test lasted. The figure shows that cracks developed sufficiently during the test to allow studying the capabilities of the device to detect cracks before they become visible.

The GPR device comes with a simple post-processing software (*StructureScan Mini* Viewer) that allows managing 2D graphical soil profiles from the data recorded, i.e. the result of the emission and subsequent collection of electromagnetic waves reflections. Among other things, the program allows setting different values of the dielectric constant to better adjust to the medium and therefore match more accurately the actual dimensions of the specimen. It is known that soils between the dry and saturated states have a dielectric constant ranging from 20 to 30 (Alharti and Lange 1987; Bridge et al. 1996; Friedman 1997, 1998; Kim and Jeong 2004; Noborio 2001). Unfortunately, because the device used was made for scanning concrete and similar materials, it could only be set for dielectric constants between 4 and 12, which distorted the dimensions of the specimen under study, enlarging its thickness during the initial post-processing. This distortion is later adjusted with a more refined post-processing.

The evolution of the specimen along path 1 is shown in Figure 5, with scans carried at days 1, 8, 15, 22 and 29 of the drying process. The sequence of images shows the expected gradual shrinkage of the specimen due to drying. Also, the profiles corresponding to days 22 and 29 contain a hyperbola that indicates the existence of an internal crack.

The profile corresponding to the first day of the test shows considerable heterogeneity. This was expected because specimens are initially in a disordered state due to the energy supplied during its fabrication and placement in the tray. Also, at this initial time, there is greater signal attenuation because the degree of saturation is at its maximum value. The handling of the specimen during the preparation stage may also contribute to cause areas or points on the soil mass capable of producing cracks during drying. The profile analysed shows that this potential tends to disappear after the first few hours. After 24 hours, a thin layer of free water forms at the surface following initial settlement and homogenisation of the specimen, and after the second day the profiles are considerably more homogeneous. The profiles corresponding to days 8 and 15 are fairly homogeneous suggesting that there are no internal cracks or significant heterogeneities in the area analysed.

An important issue for obtaining meaningful information from GPR scans is learning how to detect an internal crack. Figure 6 shows the GPR profile along horizontal path 1 and the corresponding surface image obtained at day 21, where a visible surface crack intersecting path 1 can be associated to the hyperbola on the upper right corner of the GPR profile. On the other hand, the smaller quasi-vertical crack reaching, but not crossing, path 1 is not detected because it lies outside the influence zone of the GPR electromagnetic waves.

In contrast, Figure 7 shows the profile along path 1 and surface image one day later (day 22). The smaller crack has now propagated towards the centre of the specimen, fully crossing the GPR path and therefore being detected, showing a clear new hyperbola on the upper-left corner of the profile. Thus it is clear that it is this diffraction pattern in the shape of a hyperbola that indicates the presence of a crack.

Further, Figure 8 shows the profile along path 3 and the surface image also at day 22 of the test. The intersection points of the two well-developed cracks with path 3 are closer than in path 1, resulting in two hyperbolas which are also closer.

By measuring the distance between the tips of these hyperbolas the actual distance between the cracks can be known. Therefore, the analysis of the GPR profiles allows not only detecting the presence of cracks but also measuring the distance between them, with some limitations due to the precision of the device. This limitation is illustrated in Figure 9, which shows the GPR profile along path 4 and surface image at day 22 of the test. Along this path, the cracks are separated 2.5 cm and the hyperbolas obtained with the GPR are nearly coincident in one large shape, as can be seen in the upper part of the profile, making the distinction between the two cracks impossible. The implication is that, with the current technology available, the precision does not allow discriminating between cracks that are closer than 5 cm. Another limitation is in the detection of very fine cracks. Cracks that are a few millimetres wide are easily detected but in general sub-millimetre cracks remain invisible to the GPR.

The post-processing software can show the graphical results of the tests using a variety of colour schemes, which can be useful for better interpretation of the scans. The choice of a particular colour scheme is a personal decision of the operator, who must choose it according to his/her own abilities in identifying the main features of the profile from the visual data. This ability must be trained in order to identify the main items, including cracks, that can be detected form the graphic results.

The main objective of this technique is to detect the cracks before they become visible. Therefore, it is necessary to check the ability of the device to detect cracks that form at the bottom or within the specimen before they appear on the surface. To check for that, 14 profiles corresponding to day 20, before cracks appeared on the surface of the specimen, were obtained and analysed. Of those, seven correspond to a horizontal motion of the device (paths 1 to 7) and seven correspond to a vertical motion (paths 8 to 14). Figure 10 shows those profiles on which marks have been made on suspected points where cracks might be progressing within the specimen. Figure 11a shows the location of these suspected points in plan view on an image

of the specimen's surface after 20 days of drying. The circles indicate suspected points detected during the horizontal motion of the device (paths 1 to 7), while the triangles indicate suspected points detected during the vertical motion (paths 8 to 14). Only in three of the suspected points there is coincidence between the horizontal and vertical profiles and, interestingly, at two of those points a crack appears at the surface two days later, as seen in Figure 11b which shows the same surface on day 22 of the test, with 3 cracks having become visible. The suspected point located on paths 5/9 does not lead to a surface crack on that day, however on day 28 (Figure 11c) a crack does appear on the surface very close to this area which then progresses to be of a significant size on day 36 as seen in Figure 11d.

A more detailed analysis of the results can be conducted with the dedicated software RADAN (GSSI 2009), with extended post-processing capabilities. As an example, Figure 12 shows the 14 profiles corresponding to day 22 of the test in a single view. The software allows the representation of two vertical orthogonal profiles and simultaneously, after post-processing, a horizontal slice at a chosen position to render a pseudo-3D view (Figure 13).

Figure 14 shows two particular profiles corresponding to the *x*- and *y*-directions, with a horizontal slice. This particular construction can be used to analyse the cracking state at points situated in the intersection of the two profiles, at different depths. The quality and accuracy of the graphic results can be optimized by conveniently modifying the power gain as well as the input value of the dielectric constant.

As an example, focus is turned to the main crack that develops during the test (from the upper-left to the bottom-right corners). Figure 15 shows the crack and the points of interest where the pseudo-3D images will be generated. These images, at the seven intersection points, are shown in Figure 16. The sequence shows that the crack path is detected easily from the pseudo-3D images. Figure 17 shows the final crack pattern at the end of the test as seen from the top (airside, left) and the bottom (after dismantling, right). The image of the bottom surface

shows small cracks that have not emerged to the upper surface and have been invisible to the GPR because of their small width.

Cyclic Test

This test consisted of five stages: first drying, first wetting, flooding, second drying, and second wetting with a total duration of 55 days. It was carried out in an environmental chamber (Lakshmikantha 2009) that allows for temperature and humidity cycles (Levatti 2015). The specimen was a cylinder of 80 cm in diameter and 10 cm thick. It was fully instrumented (Figure 18) with six tensiometers T5X (T1 to T6 in the Figure) to record suction in the range 100 to -200 kPa, three sensors 5TE (D1 to D3 in the Figure) to record soil temperature and volumetric water content, two Vaisala sensors (V1 and V2 in the Figure) to record relative humidity and temperature of the soil, and three load cells to record weight changes due to changes in water content. Table 4 shows the specifications of the temperature and relative humidity that were imposed during each stage of the test.

Images of the external surface were taken at regular intervals during the test. Figure 19 (first drying), Figure 20 (first wetting and flooding), Figure 21 (second drying) and Figure 22 (second wetting) show sequences of the evolution of the crack pattern on the surface of the specimen during the test. In addition to the instrument readings and the images of crack patterns, four GPR scans were made at 48, 167, 291 and 455 hours during the first two stages of drying and wetting, to check for internal cracks before they were visible on the outer surface.

Figure 23 shows the evolution of the weight of the specimen (plus the container and instrumentation) with time during the five stages of the test. The spikes at days 3, 8, 13 and 20 correspond to the effect on the load cells of the GPR scans performed on those days, which are indicated in the figure.

FIRST STAGE (FIRST DRYING, 14 DAYS)

The analysis of the weight changes recorded by the load cells shows that during the first stage approximately 12 litres of water evaporated (Figure 23). The same figure shows the times at which the GPR scans were conducted, clearly marked by an increase of weight detected by the load cells. Figure 24 shows the temperature changes in the environmental chamber. During the first hours of the test, the temperature fluctuated until it reached a steady level of 28^{o}C after about two days. From that time, the temperature inside the environmental chamber was kept at that level for the remainder of the test. No data from the sensors seems to point to the crack initiation or to their influence in the drying process.

SECOND STAGE (FIRST WETTING, 5 DAYS)

During this stage the relative humidity of the chamber's atmosphere was raised to 80%, while keeping the temperature constant at about 24^{o}C. The reason for lowering the temperature from the previous level of 28^{o}C was to check whether changing the air temperature changed significantly the soil temperature.

Figure 26 shows an inflection point in the suction measurements from the tensiometers at the time when the chamber environment was changed. The slope, almost constant, is significantly less than during the previous drying stage. This proves that the tensiometers are capable of detecting these changes and therefore allow detection of environmental changes while measuring the soil's suction.

The objective of this wetting stage was to investigate how changing the chamber's air humidity affects suction. During the few days that this stage with high relative humidity lasted no significant changes in the crack pattern was detected, regardless of the fact that the suction increased. During this stage, the loss of water in the specimen was almost negligible, showing equilibrium of water content between the soil and the environment: there seemed to be no interchange of water between the environment and the specimen. However, suction continued

increasing, probably because of internal migration of water within the soil mass, or perhaps because of the slow response of the tensiometers.

During the stage the recorded soil temperature shows a decrease that corresponds to the chamber's air temperature decrease (see Figure 24 and Figure 25), which indicates that the soil reaches thermal equilibrium with the air in a relatively short time of a few hours only.

THIRD STAGE (FLOODING, 7 DAYS)

The purpose of this stage was to simulate the impact of sudden intense precipitation on a cracked soil. To this effect, 9 litres of water were added to the partially dry specimen. This was the volume of water the cracks and container capacity permitted and was three litres short of the 12 litres that were lost during the drying stage. This difference can be explained because of the extremely long time it would take to reintroduce the full 12 litres of water into the soil pores. Figure 20 shows the flooded specimen at day 20.

During this stage, new cracks appeared, especially near the borders of cracks already present. This can be explained by the fact that, when flooding, the degree of saturation increases rapidly and the suction decreases accordingly, thus reducing the tensile strength and favouring the appearance of new cracks. The flooding conditions of humidity and temperature were maintained until no further changes of the crack pattern took place. The air relative humidity during this stage was kept at a constant 75% (see Figure 24).

FOURTH STAGE (SECOND DRYING, 12 DAYS)

The second drying stage was imposed with an air temperature of 24^{o}C and relative humidity of 30%. A comparison between the first and second drying stages shows that in order to reach a suction of 30 kPa 15 days were needed in the first stage while only 10 days were needed in the second stage (see Figure 26) even with a chamber temperature that was 4^{o}C lower. Also, the rate of suction increase at the end of this second stage was constant and considerably higher.

The first part of these drying stages, in which the suction remains constant near 0 kPa, is shorter in the first of the drying stages (7 days) than in the second (9 days). However, it must be noted that in the first drying stage, the drying temperature and humidity were imposed from the beginning, while in the second drying stage there was a transition period with higher air relative humidity. Another essential difference comes from the fact that during the first drying, the specimen was fully saturated from the beginning (all pores full of water), but in the second stage, not all pores were full of water. Also, the specimen at the start of the first drying stage did not have cracks, which is not the case for this second stage.

An interesting fact is that because of flooding the specimen experiences considerable degradation, with new cracks developing close to the previous ones. This shows that cracking is irreversible at least for short time periods.

FIFTH STAGE (SECOND WETTING, 17 DAYS)

Once the specimen reached a dry condition more intense than in the first stage, the chamber relative humidity was raised again to 75%, and the temperature was set to 22^{o}C. These values were kept until the end of the 55 days. The readings of the tensiometers (Figure 26) show how suction slowly decreases because of the new environmental conditions. Figure 25 shows how the specimen reaches thermal equilibrium, with decreasing soil temperature that approaches the air temperature.

GPR SCANS (DAYS 3, 8, 13 AND 20)

The GPR technique described in previous sections has been used to analyse the possible development of internal cracking during this test. The device has been able to detect the presence of the sensors at their respective position as well as other possible crack-initiating elements during the test.

Figure 27 shows the grid used during the days 3, 8, 13 and 20 to obtain the readings. The first visible crack on the top was produced on day 9 (Figure 19), in consequence the only information about internal cracks before day 9 comes from the GPR readings. The grid on days 13, 20 and at the final stage of the cyclic test (Figure 27), permits to establish the relation within crack development and GPR profiles. Four cracks (crack 1, crack 2, crack 3 and crack 4), which appeared in chronological order during the drying stages, are identified in order to analyse the GPR readings.

Figure 28 (paths 1 to 6) and Figure 29 (paths 7 to 14) show the GPR profiles obtained on days 3, 9, 13 and 20. Path 1 of day 3 shows, marked with a circle, what can be interpreted as a crack. However, this signal disappears in later profiles on days 8, 13 and 20. This was probably only a momentary discontinuity in the specimen's mass or a momentary heterogeneous distribution of water. Paths 2 and 3 show no cracks during the four days of auscultation. However, it is clear that the distribution of water is not totally homogeneous and the specimen's vertical shrinkage is detected as in the drying test (see previous section).

Path 4 shows clearly the central tensiometer T3 on the four days and a signal that can be interpreted as a crack at the beginning of the path, from day 3 onwards. This crack can be the origin of crack 3 in Figure 27 that is visible on the external surface of the specimen on day 16 (Figure 20). Paths 5 and 6 show no cracks for each of the four GPR scans.

Path 7 (Figure 29) shows a crack that evolves from the middle height of the specimen (day 3) close to the end of the path, propagating towards the surface (on day 20) that seems to be the origin of crack 2 in Figure 27. Path 8 on day 20 shows crack 1 which on that day is already visible on the external surface of the specimen. Path 9 shows an internal crack that was not visible yet on the external surface. This crack evolved only partially from the bottom of the specimen and did not reach the external surface. Paths 10, 13 and 14 show no cracks for each of the four GPR scans but the profiles show heterogeneity probable produced by the three

tensiometers T3, T4 and T6 which were aligned with these paths. Path 11 shows the central tensiometer T3 and path 12 shows tensiometers T4 and T3 in the four GPR profiles, more clearly on day 3.

It is clear that the GPR is capable to detect the presence of the sensors. However, the presence of the sensors interferes with the main purpose of the GPR, which is to detect cracks. Therefore, it is recommended, if possible, to avoid placing sensors in the area where GPR scans will take place during testing.

Conclusions

The ground penetrating radar system described in this paper is a promising tool for non-destructive indirect detection of crack formation and propagation within a drying soil mass by allowing a more comprehensive monitoring of the internal cracks. The interpretation of the results is complex and requires acquired skill of the analyst, because the GPR use in soil cracking has to be adapted from its original, non-geotechnical, purpose to the soil's particular characteristics, in particular to the fact that its electromagnetic properties do not remain constant over time due to the changes of its constituents. The ability of the analyst in identifying the main features of the cracking process from visual observation of the profiles is fundamental and requires considerable training involving not only visual ability, but also knowledge of the technical workings of the device and the software, so that adjustments can be made in all stages of the test: specimen design; definition of the scanner paths grid; and post-processing.

Regardless of some limitations, the GPR system is sensitive to changes in water content that occurs in the soil during desiccation. Cracks with crack width larger than 1 to 2 mm are easily detected, while thinner cracks are not identified with the currently available devices. The separation between cracks when the distance is more than about 5 cm can also be obtained from the GRP profiles. However, cracks that are closer than 5 cm create interferences in the profile, thus preventing the correct interpretation of the data. Given the continuous technical

evolution of GRP devices, it is envisioned that with higher wave frequencies the resolution will improve significantly, thus allowing detection of thinner cracks and identification of the separation between them. For this to occur, of course, the industry must develop these higher-frequency devices, as the need for them increases and makes their development profitable.

A key advantage of the GPR technique is its low cost when compared to other systems such as X-rays, CT scans or MRIs. The GPR device is much less expensive and fully portable. Its ease of use and continuous evolution makes it a good choice to work both in the field and in the laboratory and, when combined with currently available systems to study cracking in soils, can greatly improve the prediction and understanding of how shrinking of soils induce cracks, and how those cracks later propagate.

The cyclic test presented shows that cycles of wetting and flooding in addition to drying have a strong influence on the variables that govern the cracking phenomenon. Flooding produces additional cracks on the specimen, after drying and wetting, showing the irreversibility of cracking for the duration of the test.

Acknowledgements

Financial support from research grant BIA2012-36498, awarded by the Spanish Ministry of Economy and Competitiveness (including FEDER funds, European Commission) is gratefully acknowledged. The first author wishes to thank the support of the ASTUTE Project, College of Engineering, Swansea University.

References

Alharti, A., and Lange, J., 1987, "Soil water saturation: dielectric determination," *Water Resources Research*, Vol. 23, pp. 591-595.

Ávila, G., 2004, "Estudio de la retracción y el agrietamiento de arcillas. Aplicación a la arcilla de Bogotá," Ph.D. Thesis, Dept. of Geotechnical Engineering and Geosciences, UPC-BarcelonaTech.

Barrera, M., 2002, "Estudio experimental del comportamiento hidro-mecánico de suelos colapsables," Ph.D. Thesis, Dept. of Geotechnical Engineering and Geosciences, UPC-BarcelonaTech.

Brandes, I. M., 2005, "The negative chargeability of clays," Ph.D. Thesis, School of Civil and Environmental Engineering, University of New South Wales, Australia.

Bridge, B. J., Sabburg, J., Habash, K. O., Ball, J. A. R., and Hancock, N. H., 1996, "The dielectric behaviour of clay soils and its application to time domain reflectometry," *Australian Journal of Soil Research*, Vol. 34, pp. 825-835.

Chertkov, V. Y., 2002, "Modelling cracking stages of saturated soils as they dry and shrink," *European Journal of Soil Science*, Vol. 53, pp. 105-118.

Cordero, J., Cuadrado, A., Ledesma, A., and Prat, P. C., 2014, "Patterns of cracking in soils due to drying and wetting cycles," *6th International Conference on Unsaturated Soils, UNSAT 2014*, Sydney, Taylor and Francis, pp. 381-387.

Corte, A., and Higashi, A., 1960, *Experimental research on desiccation cracks in soil,* Report 66, Corps of Engineers, US Army Snow, Ice and Permafrost Research Establishment, Wilmette, Illinois, USA.

Friedman, S. P., 1997, "Statistical mixing model for the apparent dielectric constant of unsaturated porous media," *Soil Science Society of America Journal*, Vol. 61, No. 3, pp. 742-745.

Friedman, S. P., 1998, "A saturation degree-dependent composite spheres model for describing the effective dielectric constant of unsaturated porous media," *Water Resources Research*, Vol. 34, No. 11, pp. 2949-2961.

GSSI. 2009, "RADAN® Manual," Geophysical Survey Systems, Inc., Salem, NH, USA.

Haines, W., 1923, "The volume-changes associated with variations of water content in soil," *Journal of Agricultural Science*, Vol. 13, pp. 296-310.

Hassan, A., and Toll, D. G., 2013, "Electrical resistivity tomography for characterizing cracking of soils," *ASCE Geotechnical Special Publication*, Vol. 231, pp. 818-827.

Hu, L. B., Hueckel, T., Péron, H., and Laloui, L., 2008, "Modeling Evaporation, Shrinkage and Cracking of Desiccating Soils," *IACMAG 12*, Goa, India, IIT Mumbai, pp. 1083-1090.

Jahn, A., 1950, "Peculiar polygonal markings on the meadows in the Wieprz river valley," *Acta Geologica Polonica*, Vol. 1, No. 2, pp. 150-157.

Kim, M. I., and Jeong, G. C., 2004, "A study on the determination of dielectric constant of saturated porous media using frequency domain reflectometry system," *J. Eng. Geol.*, Vol. 14, No. 2, pp. 179-187.

Knechtel, M. M., 1952, "Pimpled plains of Eastern Oklahoma," *Bulletin of the Geological Society of America*, Vol. 63, pp. 689-700.

Knoll, M. D., and Knight, R., 1994, "Relationships between dielectric and hydrogeologic properties of sand-clay mixtures," *Fifth International Conference on Ground Penetrating Radar*, Waterloo Centre for Groundwater Research, pp. 45-61.

Kodikara, J., Barbour, S. L., and Fredlund, D. G., 2000, "Desiccation cracking of soil layers," *Unsaturated Soils for Asia*, Balkema, pp. 693-698.

Kodikara, J. K., Nahlawi, H., and Bouazza, A., 2004, "Modelling of curling in desiccation clay," *Canadian Geotechnical Journal*, Vol. 41, pp. 560-566.

Lachenbruch, A. H., 1961, "Depth and spacing of tension cracks," *Journal of Geophysical Research*, Vol. 66, No. 12, pp. 4273-4292.

Lakshmikantha, M. R., 2009, "Experimental and theoretical analysis of cracking in drying soils," Ph.D. Thesis, Dept. of Geotechnical Engineering and Geosciences, UPC-BarcelonaTech.

Lakshmikantha, M. R., Prat, P. C., and Ledesma, A., 2006, "An experimental study of cracking mechanisms in drying soils," *Environmental Geotechnics V*, H. R. Thomas, ed., Thomas Telford, London, pp. 533-540.

Lakshmikantha, M. R., Prat, P. C., and Ledesma, A., 2009, "Image analysis for the quantification of a developing crack network on a drying soil," *Geotechnical Testing Journal*, Vol. 32, No. 6, pp. 505-515.

Lakshmikantha, M. R., Prat, P. C., and Ledesma, A., 2012, "Experimental evidences of size-effect in soil cracking," *Canadian Geotechnical Journal*, Vol. 49, No. 3, pp. 264-284.

Lakshmikantha, M. R., Prat, P. C., and Ledesma, A., 2013a, "Evidences of hierarchy in cracking of drying soils," *ASCE Geotechnical Special Publication*, Vol. 231, pp. 782-789.

Lakshmikantha, M. R., Prat, P. C., and Ledesma, A., 2016, "Desiccation of Thin Soil layers: Effect of Boundary Conditions," *Geoderma (submitted - under review)*.

Lakshmikantha, M. R., Reig, R., Prat, P. C., and Ledesma, A., 2013b, "Origin and mechanism of cracks seen at the bottom of a desiccating soil specimen," *ASCE Geotechnical Special Publication*, Vol. 231, pp. 790-799.

Lambe, T., 1958, "The structure of compacted clay," *Journal of the Soil Mechanics and Foundations Division*, Vol. 84, No. 2, pp. 1-34.

Lau, J. T. K., 1987, "Desiccation cracking of clay soils," M.S. Thesis, Dept. of Civil Engineering, University of Saskatchewan, Canada.

Levatti, H. U., 2015, "Estudio experimental y análisis numérico de la desecación en suelos arcillosos," Ph.D. Thesis, Dept. of Geotechnical Engineering and Geosciences, UPC-BarcelonaTech.

Longwell, C. R., 1928, "Three commontypes of desert mud cracks," *American Journal of Science*, Vol. 15, pp. 136-145.

Mitchell, J. K., 1993, *Fundamentals of soil behaviour*, John Wiley & Sons, Inc.

Morris, P. H., Graham, J., and Williams, D. J., 1992, "Cracking in drying soils," *Canadian Geotechnical Journal*, Vol. 29, pp. 263-277.

Morrison, F., and Gasperikova, E., 2015, "The Berkeley Course in Applied Geophysics," The University of California, http://appliedgeophysics.berkeley.edu/.

Mukunoki, T., Otani, J., Maekawa, A., Camp, S., and Gourc, J. P., 2010, "Investigation of crack behavior on cover soils at landfill using X-ray CT," *Advances in X-ray Tomography for Geomaterials*, J. Desrues, G. Viggiani, and P. Bésuelle, eds., John Wiley & Sons, pp. 213-219.

Nahlawi, H., and Kodikara, J., 2006, "Laboratory experiments on desiccation cracking of thin soil layers," *Geotechnical and Geological Engineering*, Vol. 24, No. 6, pp. 1641-1664.

Noborio, K., 2001, "Measurement of soil water content and electrical conductivity by time domain reflectometry: a review," *Computers and Electronics in Agriculture*, Vol. 31, pp. 213-237.

Otani, J., and Obara, Y., 2004, "X-ray CT for geomaterials: Soils, Concrete, Rocks," Swets & Zeitlinger.

Pérez, V., 2001, "Radar de subsuelo. Evaluación para aplicaciones en arqueología y en patrimonio histórico-artístico," Ph.D. Thesis, UPC-BarcelonaTech.

Péron, H., Hueckel, T., Laloui, L., and Hu, L. B., 2009, "Fundamentals of desiccation cracking of fine-grained soils: experimental characterisation and mechanisms identification," *Canadian Geotechnical Journal*, Vol. 46, No. 10, pp. 1177-1201.

Prat, P. C., Ledesma, A., Cuadrado, A., and Levatti, H. U., 2013, "Ground penetrating radar system for detection of desiccating cracks in soils," *ComGeo-III*, Kraków, Poland, International Centre for Computational Engineering, pp. 249-258.

Rodríguez, R. L., Sánchez, M. J., Ledesma, A., and Lloret, A., 2007, "Experimental and numerical analysis of a mining waste desiccation," *Canadian Geotechnical Journal*, Vol. 44, pp. 644-658.

Samoulian, A., Cousin, I., Richard, G., Bruand, A., and Tabbagh, A., 2003, "Electrical resistivity imaging for detecting soil cracking at the centimetric scale," *Soil Science Society of America Journal*, Vol. 67, No. 5, pp. 1319-1326.

Simpson, W. E., 1936, "Foundation experience with clay in Texas," *Civil Engineering*, Vol. 4, pp. 581-584.

Skempton, A. W., and Northey, R. D., 1952, "The sensitivity of clays," *Géotechnique*, Vol. 3, No. 1, pp. 100-106.

Tang, C.-S., Shi, B., Liu, C., Gao, L., and Inyang, H., 2011, "Experimental Investigation of the Desiccation Cracking Behavior of Soil Layers during Drying," *Journal of Materials in Civil Engineering*, Vol. 23, No. 6, pp. 873-878.

Vogel, H. J., Hoffmann, H., and Roth, K., 2005, "Studies of crack dynamics in clay soil. I: Experimental methods, results and morphological quantification," *Geoderma*, Vol. 125, No. 3-4, pp. 203-211.

White, W. A., 1961, "Colloid phenomena in sedimentation of argillacious rocks," *Journal of Sedimentary Petrology*, Vol. 31, pp. 560-570.

Willden, R., and Mabey, D. R., 1961, "Giant desiccation fissures on the Black Rock and Smoke Creek deserts, Nevada," *Science*, Vol. 133, pp. 1359-1360.

TABLES

Table 1 – Electromagnetic parameters and wave propagation characteristics in air and water

Material	ε_r	σ (mS/m)	μ_r	v (cm/ns)	Γ (dB/m)
Air	1	0	1.0003	30	0
Distilled water	—	0.01	—	—	0.002
Freshwater	80 – 81	0.1 – 10	1	3.3	0.1 – 0.18
Seawater	81 – 88	4000	—	—	330 – 1000
Polar snow	1.4 – 3	—	1	19.4 – 25.2	—
Polar ice	3 – 3.15	0.02 – 0.003	—	16.8	0.01
Tempered ice	3.2	$5.10^{-4} – 8.10^{-6}$	—	16.7	0.01
Pure ice	3.2	—	—	16.7	0.01
Freshwater lake ice	4	—	—	15	0.01
Sea ice	2.5 – 8	—	—	7.8 – 15.7	—
Permafrost	1 – 8	1 – 0.1	1	10.6 – 30	—

Table 2 – Electromagnetic properties of soil components: dielectric constant (k); electrical conductivity ($\boldsymbol{\sigma}$); propagation velocity ($\boldsymbol{v}$); attenuation coefficient ($\boldsymbol{\alpha}$)

Material	k	σ (mS/m)	v (m/ns)	α (dB/m)
Air	1	0	0.3	0
Distilled Water	80	0.01	0.033	2000
Fresh Water	80	0.5	0.033	0.1
Seawater	80	3000	0.01	103
Dry Sand	3-5	0.01	0.15	0.01
Saturated Sand	20-30	0.1-1	0.06	0.03-0.3
Siltstone	4-8	0.5-2	0.12	0.4-1
Shale	5-15	1-100	0.09	1-100
Silt	5-30	1-100	0.07	1-100
Clay	5-40	2-1000	0.06	1-300
Granite	4-8	0.01-1	0.13	0.01-1
Dry Salt	5-6	0.01-1	0.13	0.01-1
Ice	3-4	0.01	0.16	0.01

Table 3 – Technical specifications of the *StructureScan Mini* device

Centre Frequency	1600 MHz
Depth Range	< 50 cm
Unit Weight	1.6 kg
Dimensions	152 by 178 by 229 (mm)

Table 4 – Specifications of temperature and relative humidity during the cyclic test

Stage	Duration (days)	Temperature (^{o}C)	Relative Humidity (%)
1 First drying	14	28	30
2 First wetting	5	24	80
3 Flooding	7	24	85
4 Second drying	12	24	30
5 Second wetting	17	22	75

FIGURES

Figure 1 – The GSSI® *StructureScan Mini* device

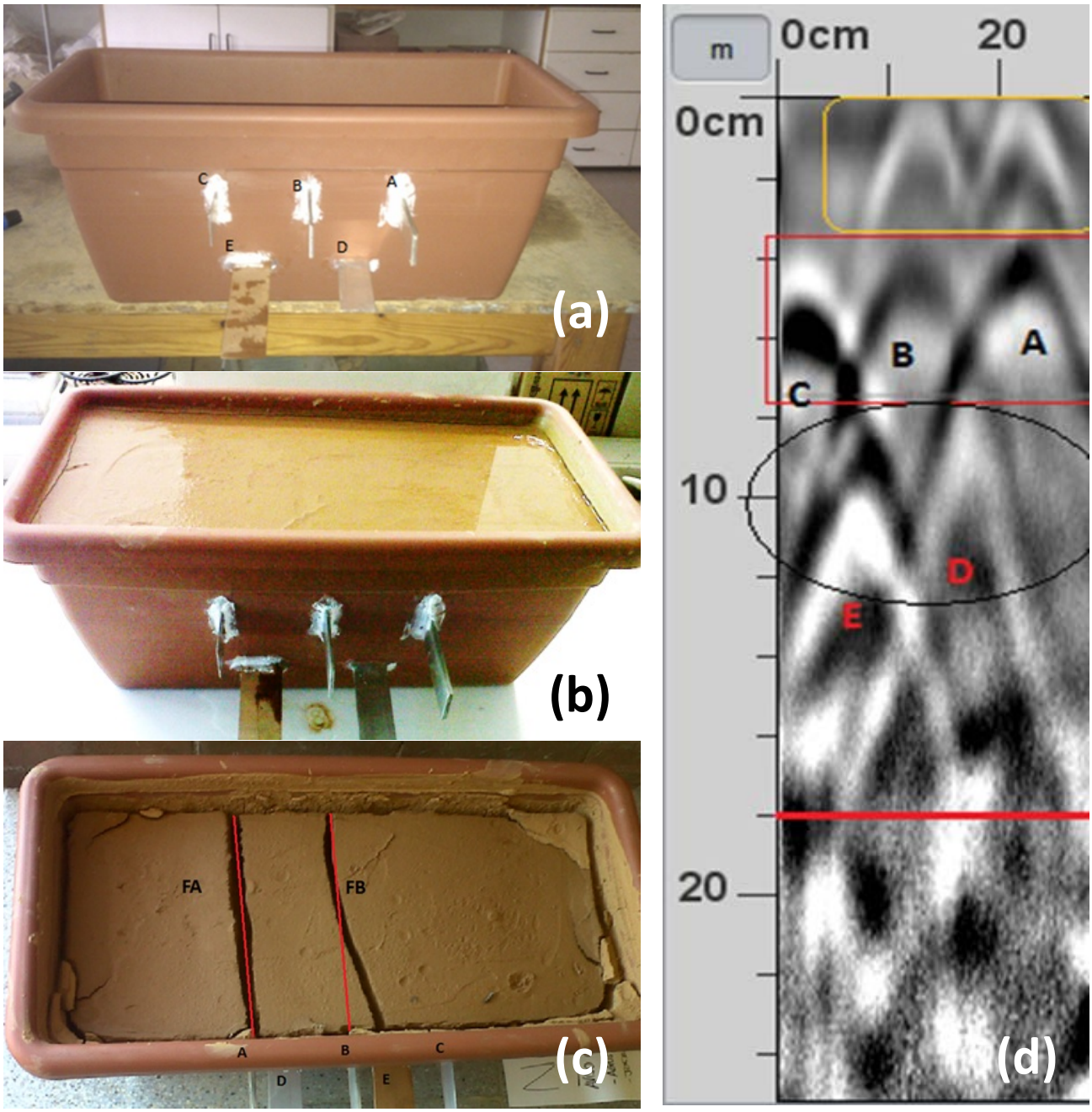

Figure 2 – Block test: (a) mould with strips inserted; (b) after pouring slurry; (c) surface cracks at 30 days; (d) GPR profile shortly after the first cracks were visible on the external surface

Figure 3 – Specimen and PMMA plate with grid to guide the device

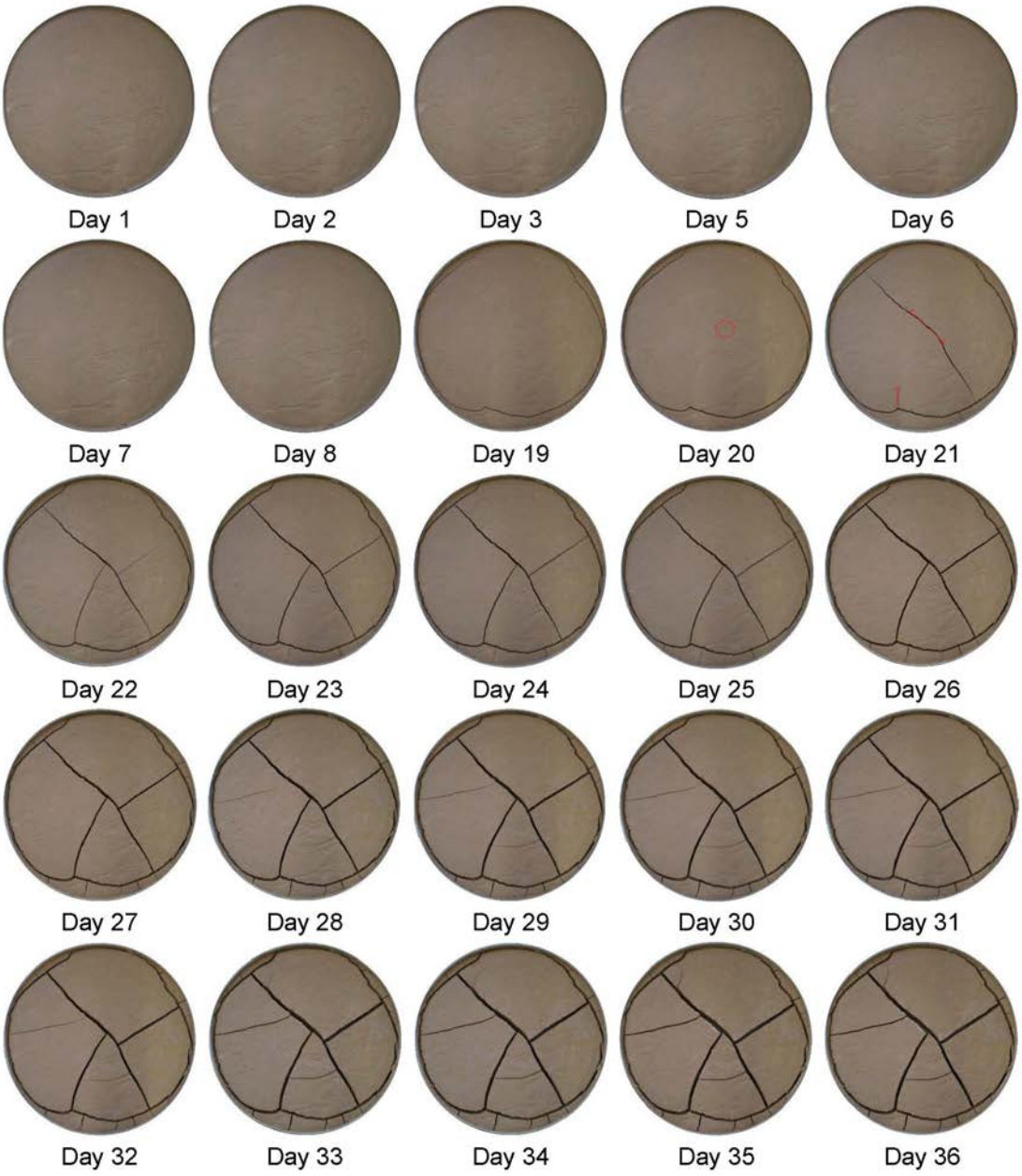

Figure 4 – Evolution of the specimen surface during 36 days of desiccation

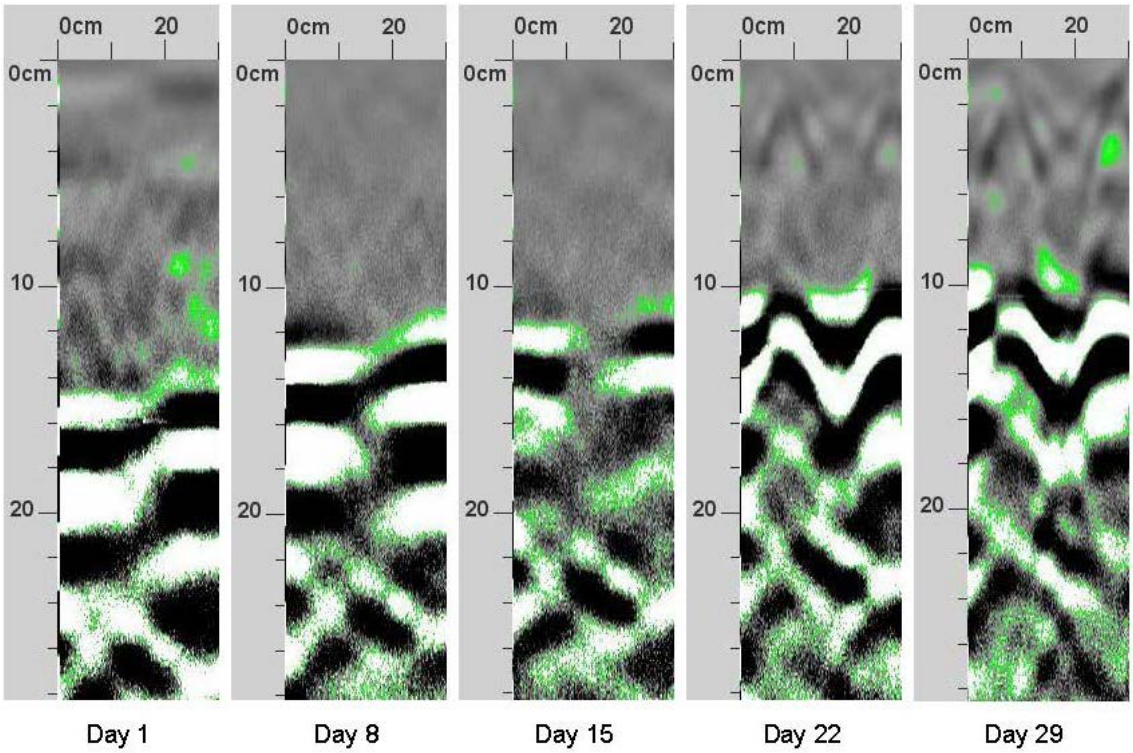

Figure 5 – Evolution of a sample profile at days 1, 8, 15, 22 and 29

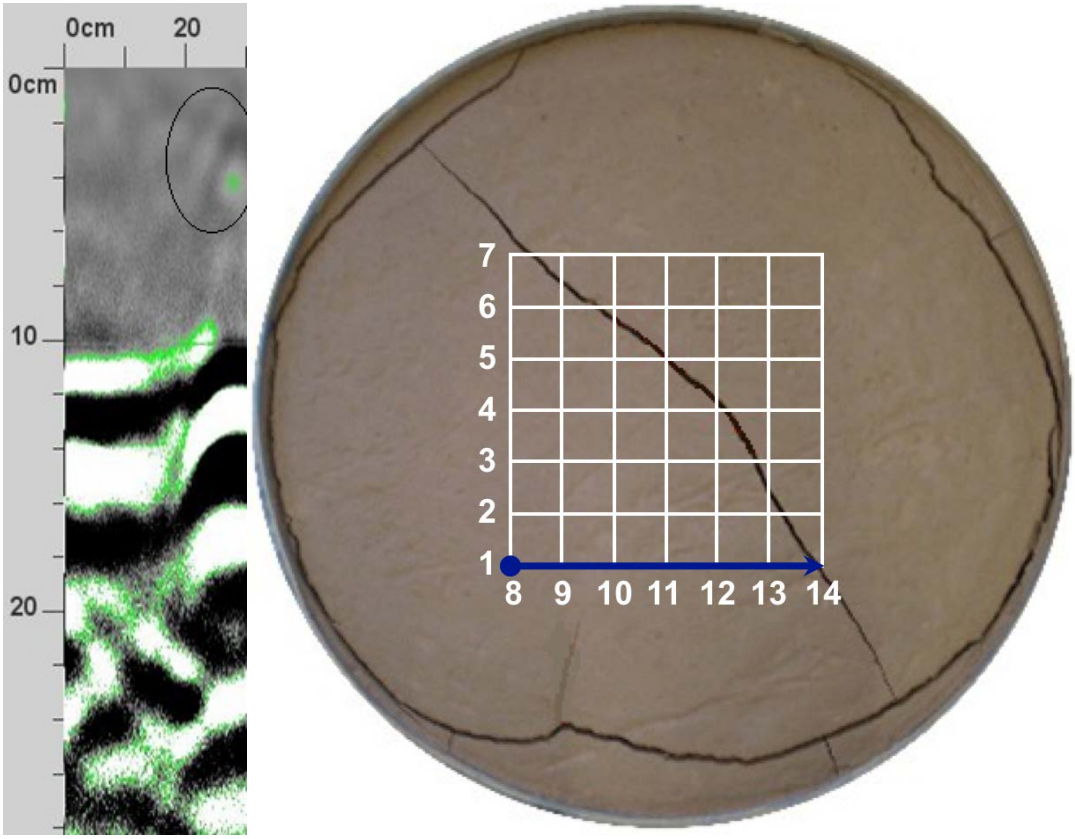

Figure 6 – GPR profile on path 1 – day 21 of desiccation test

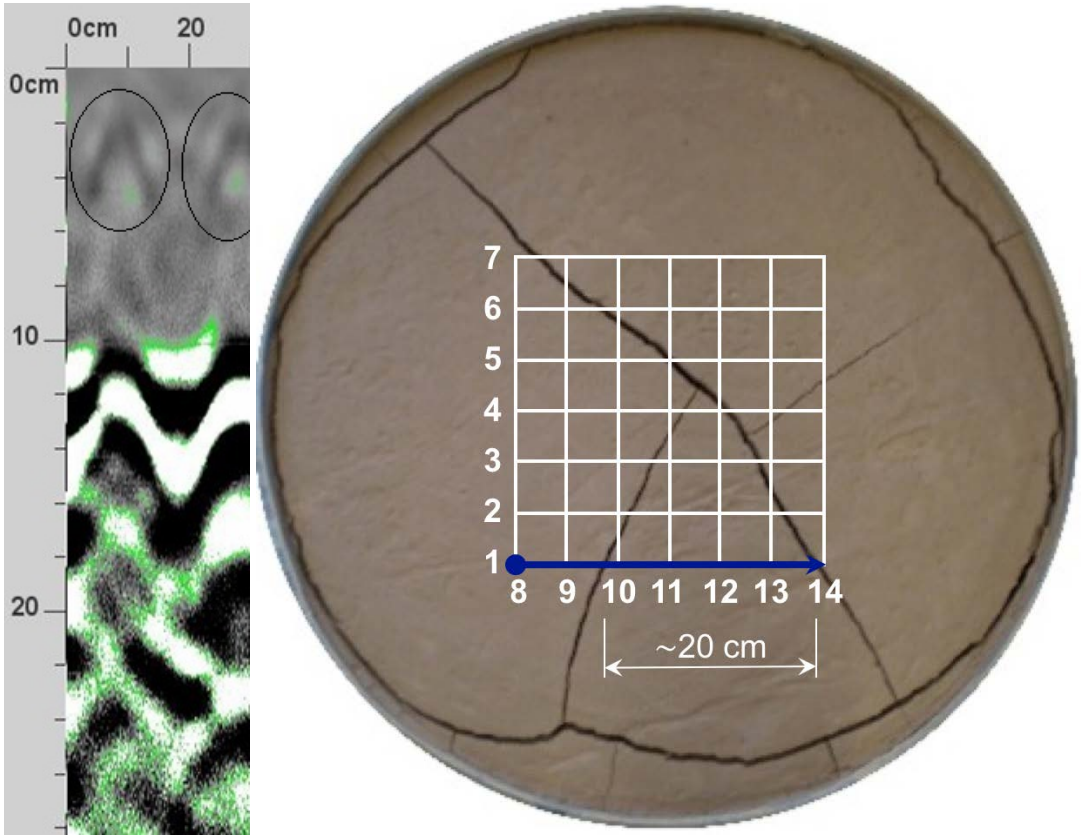

Figure 7 – GPR profile on path 1 – day 22 of desiccation test

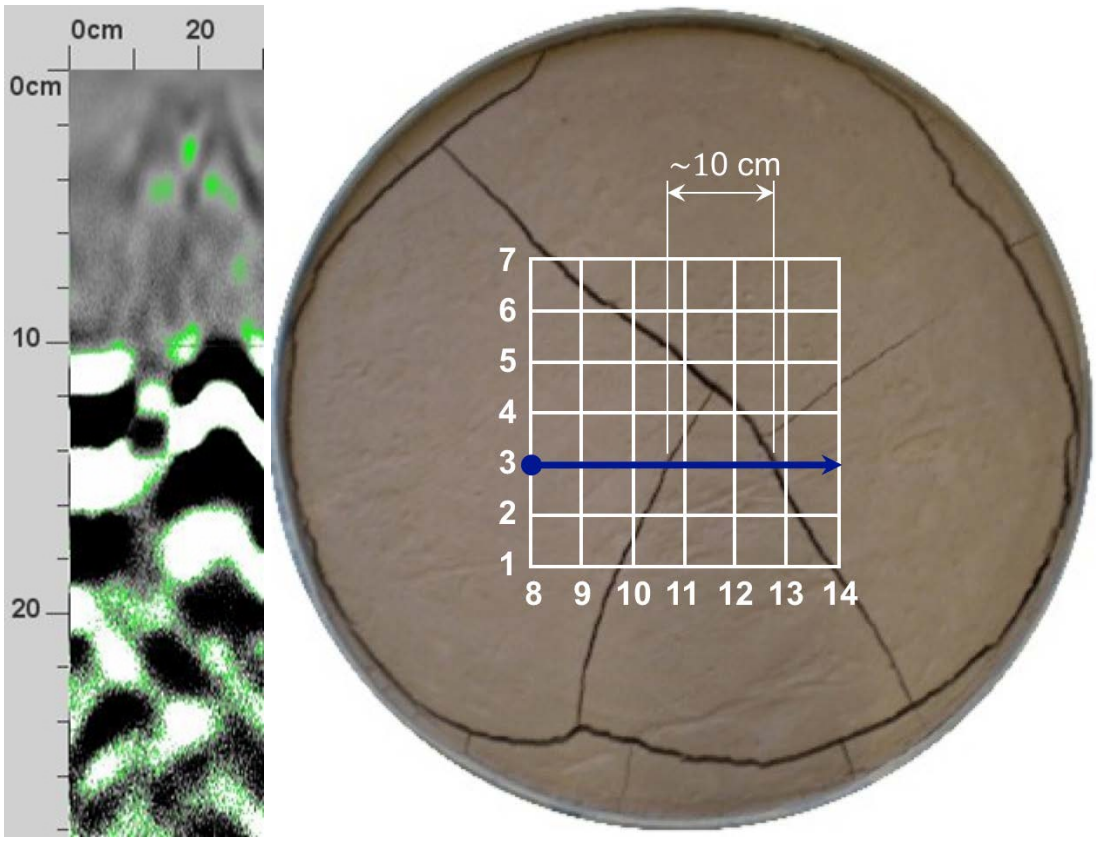

Figure 8 – GPR profile on path 3 – day 22 of desiccation test

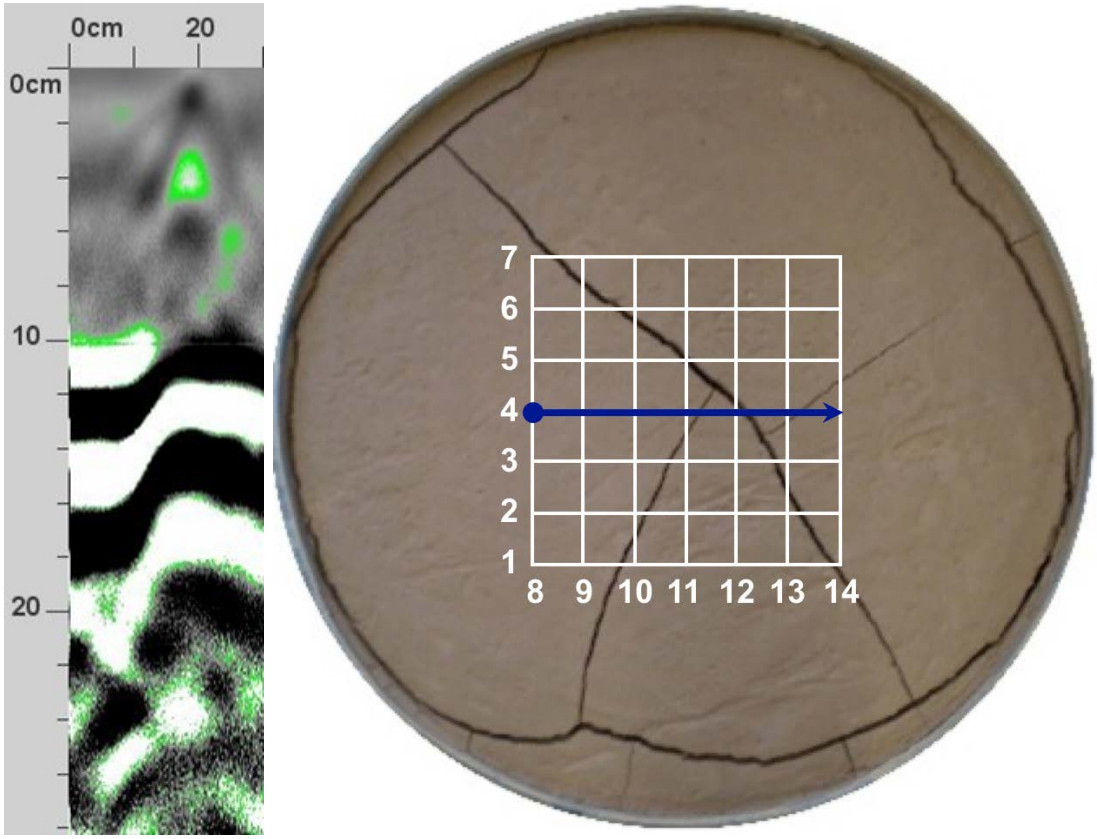

Figure 9 - GPR profile on path 4 – day 22 of desiccation test

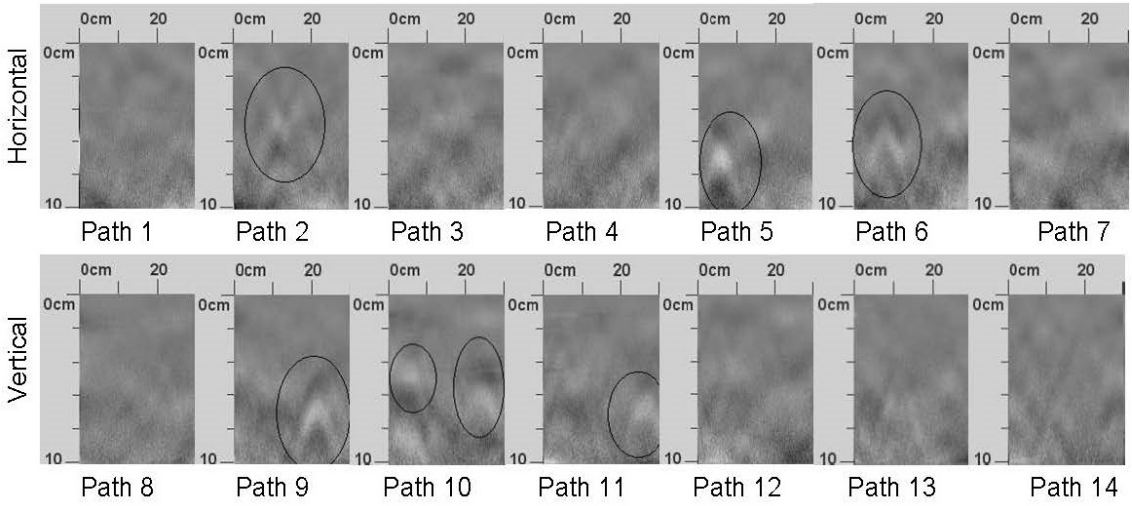

Figure 10 – GPR profiles on day 20

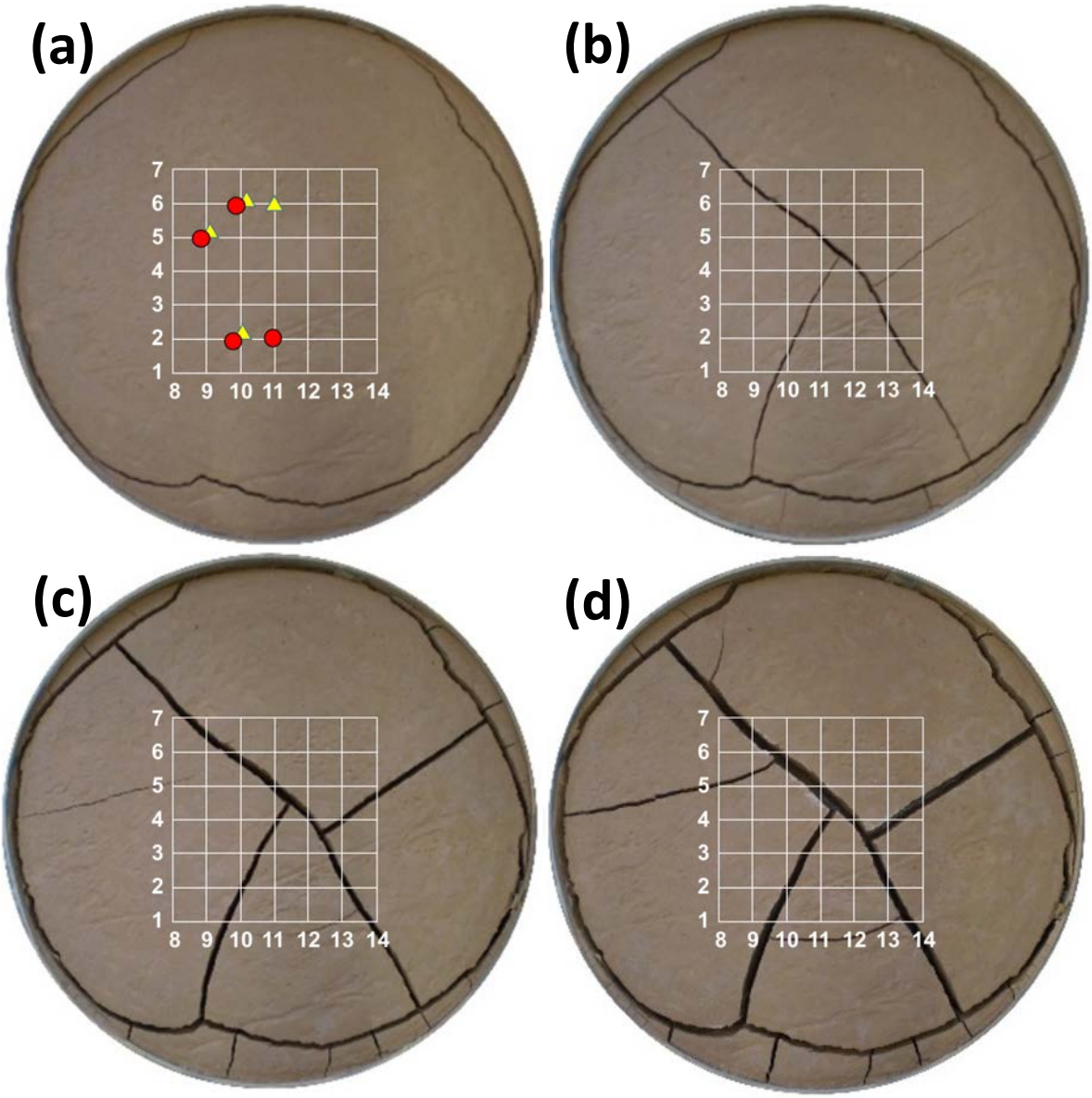

Figure 11 – (a) suspected cracks on day 20 from GPR (▲ = vertical motion, ● = horizontal motion), and (c-d) visible cracks on days 22, 28 and 36 respectively

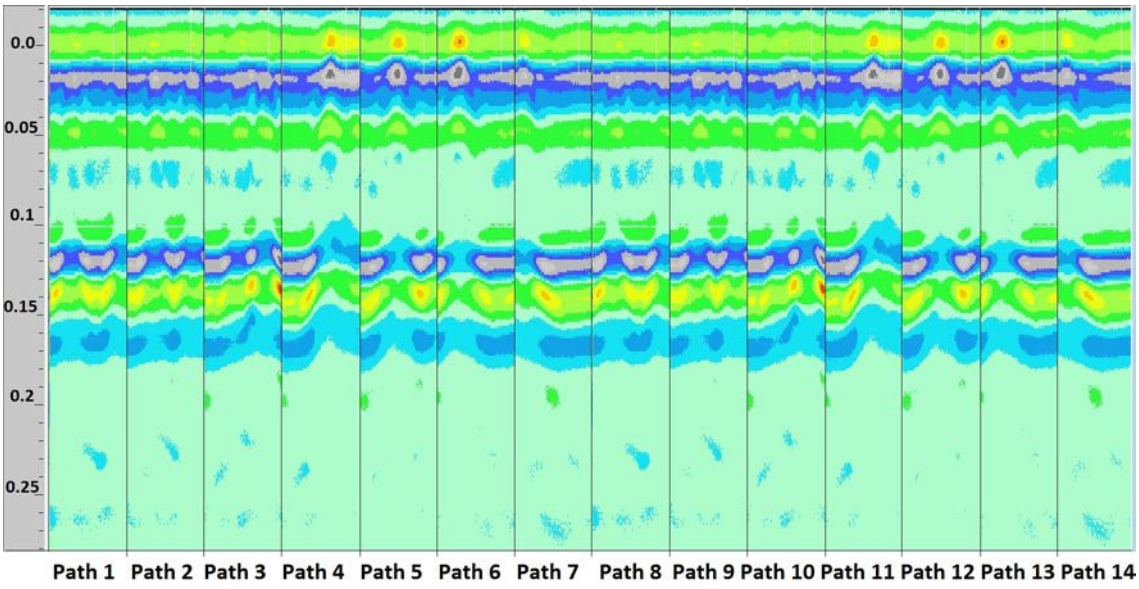

Figure 12 – GPR profiles on day 22 from the 3D analysis using RADAN 6.6

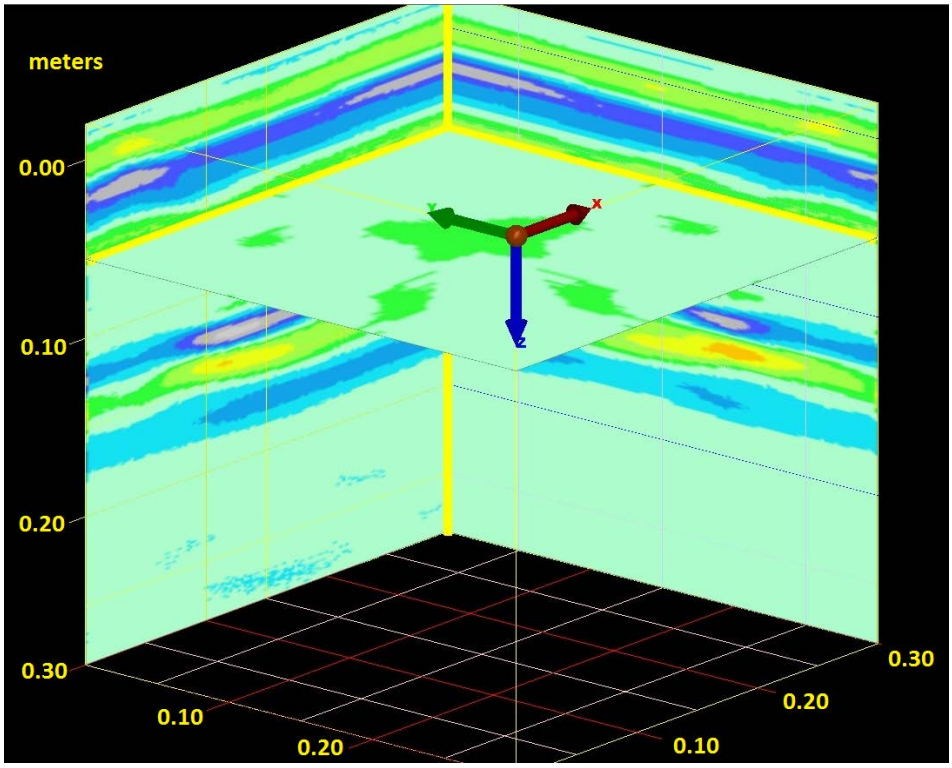

Figure 13 - Pseudo 3D obtained by RADAN 6.6

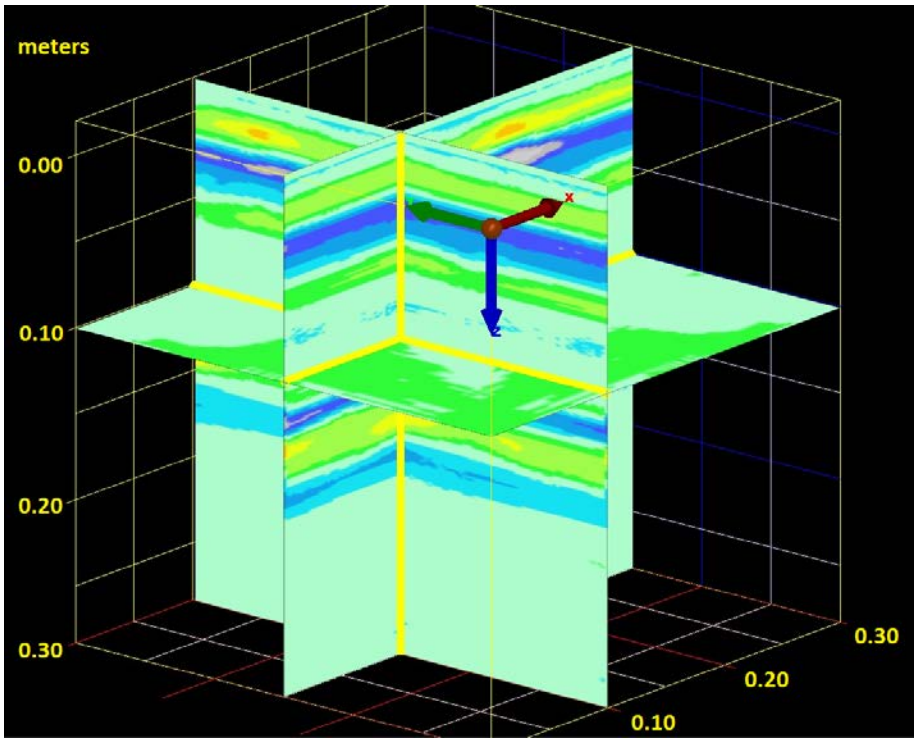

Figure 14 – Perpendicular profiles from RADAN 6.6 post-process

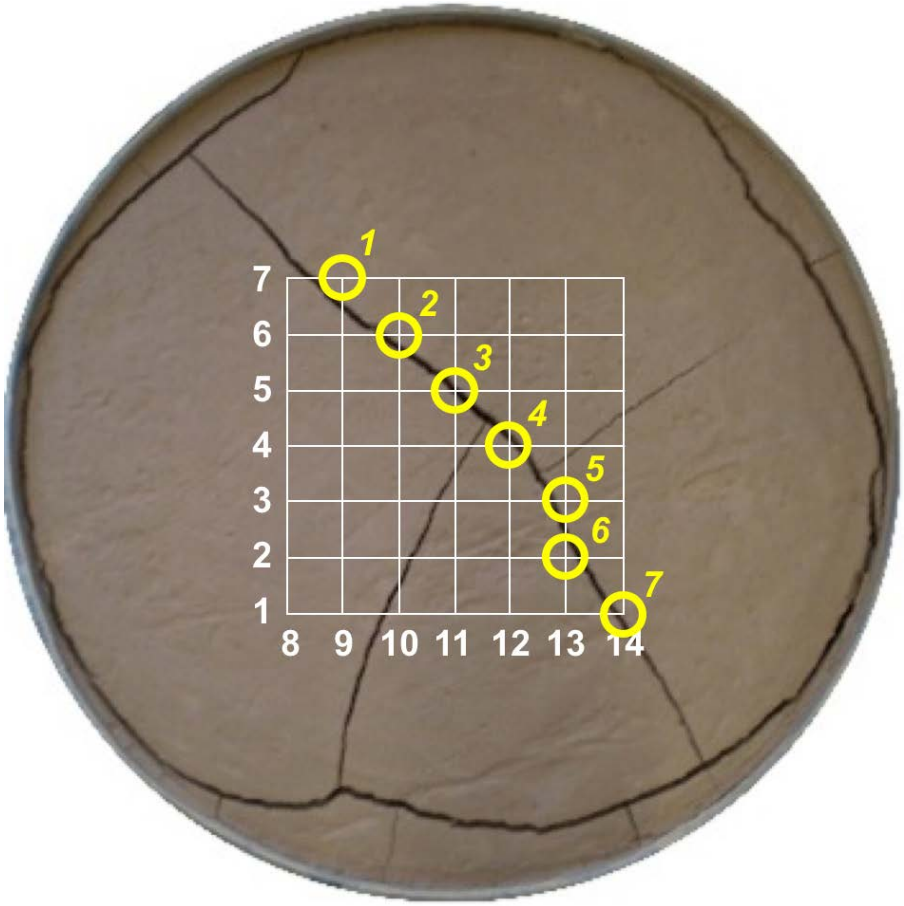

Figure 15 – Intersections at which the pseudo-3D images are obtained

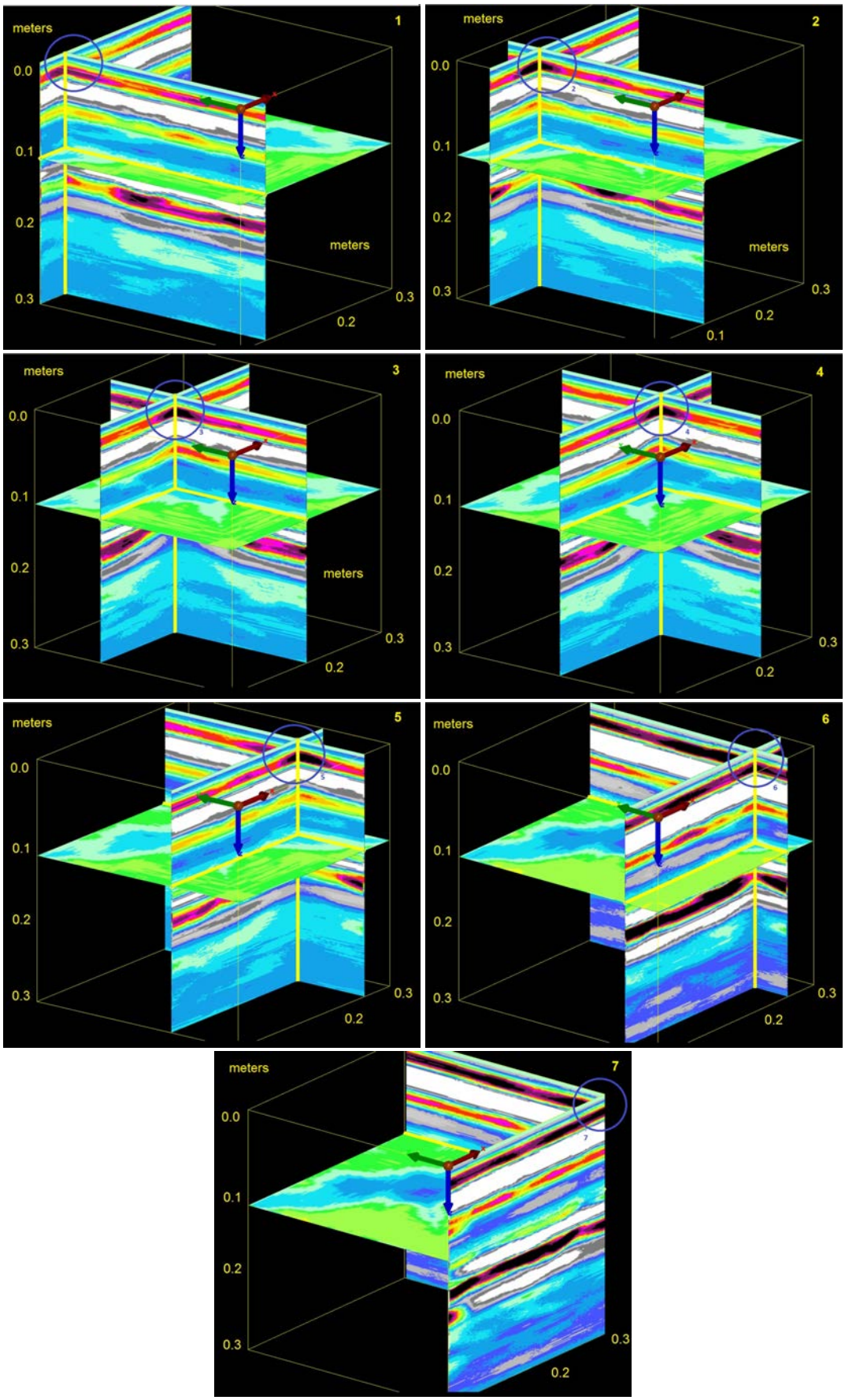

Figure 16 – Pseudo-3D images at the intersections shown in Figure 15

Figure 17 – Final crack patterns at the end of the test

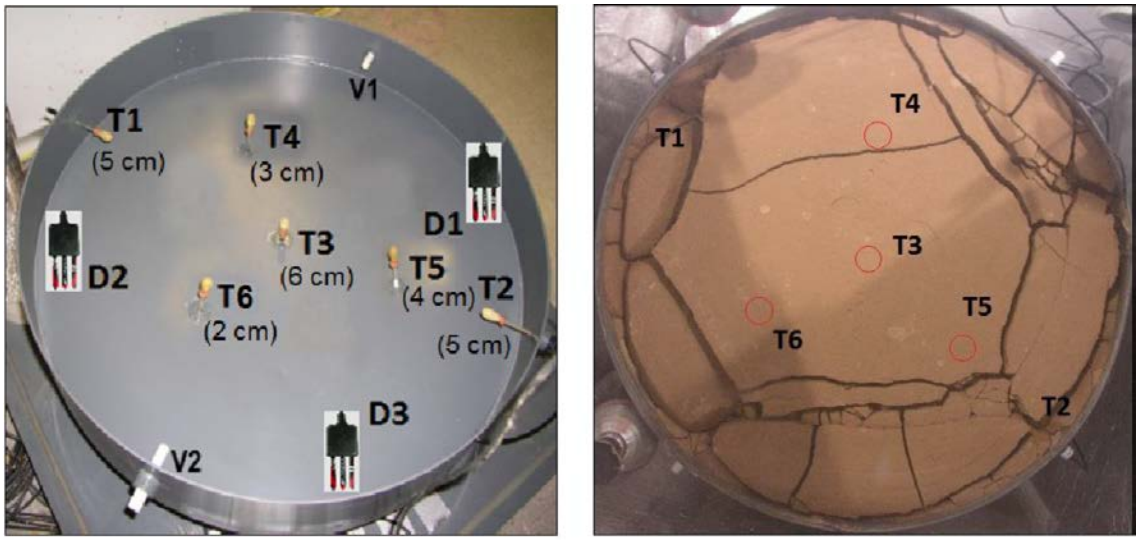

Figure 18 – Instrumentation of the soil specimen for the cyclic test: a) tensiometers T1-T6, Decagon sensors D1-D3; b) relative position of tensiometers at the end of the test

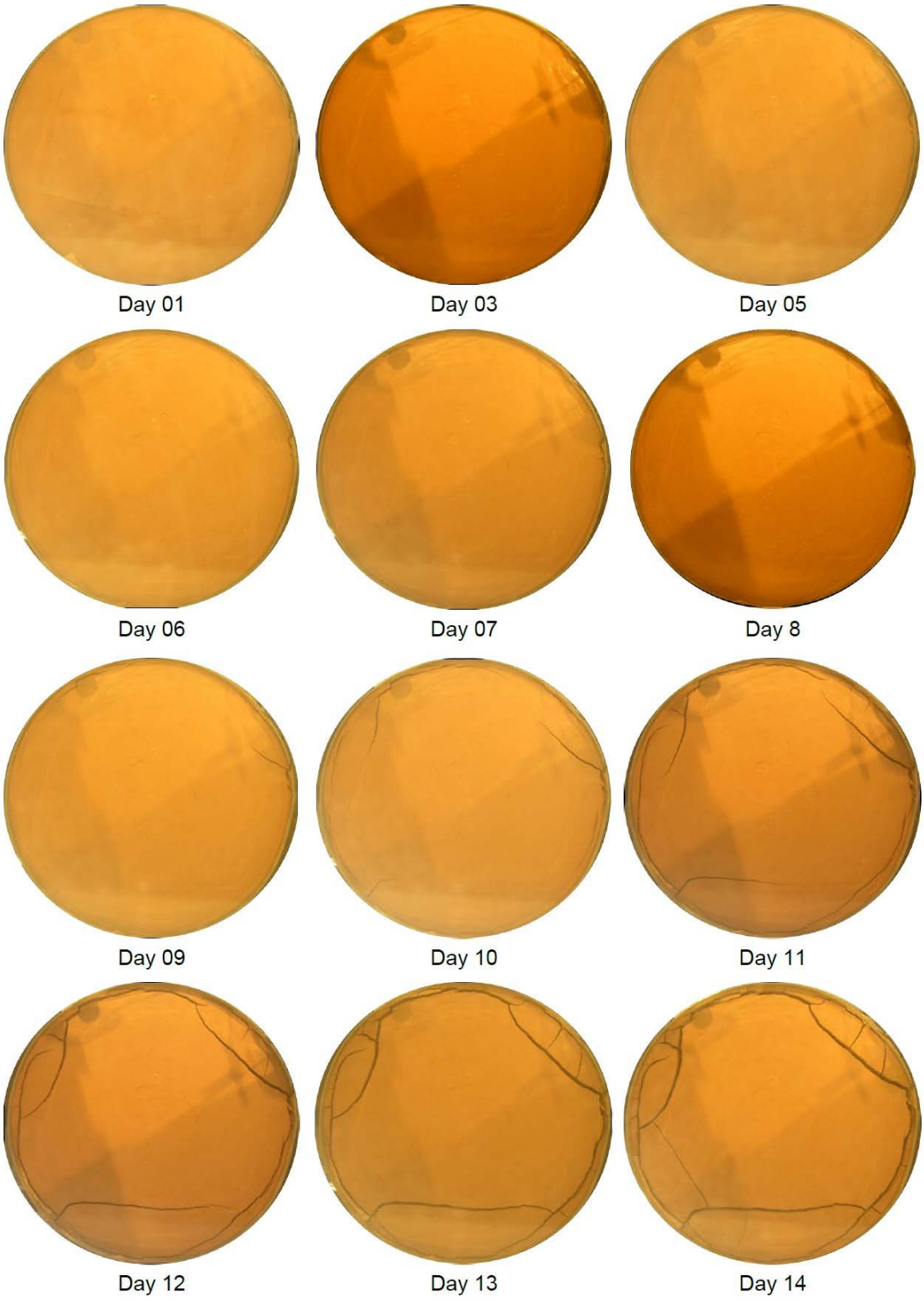

Figure 19 – Sequence showing the first stage: first drying

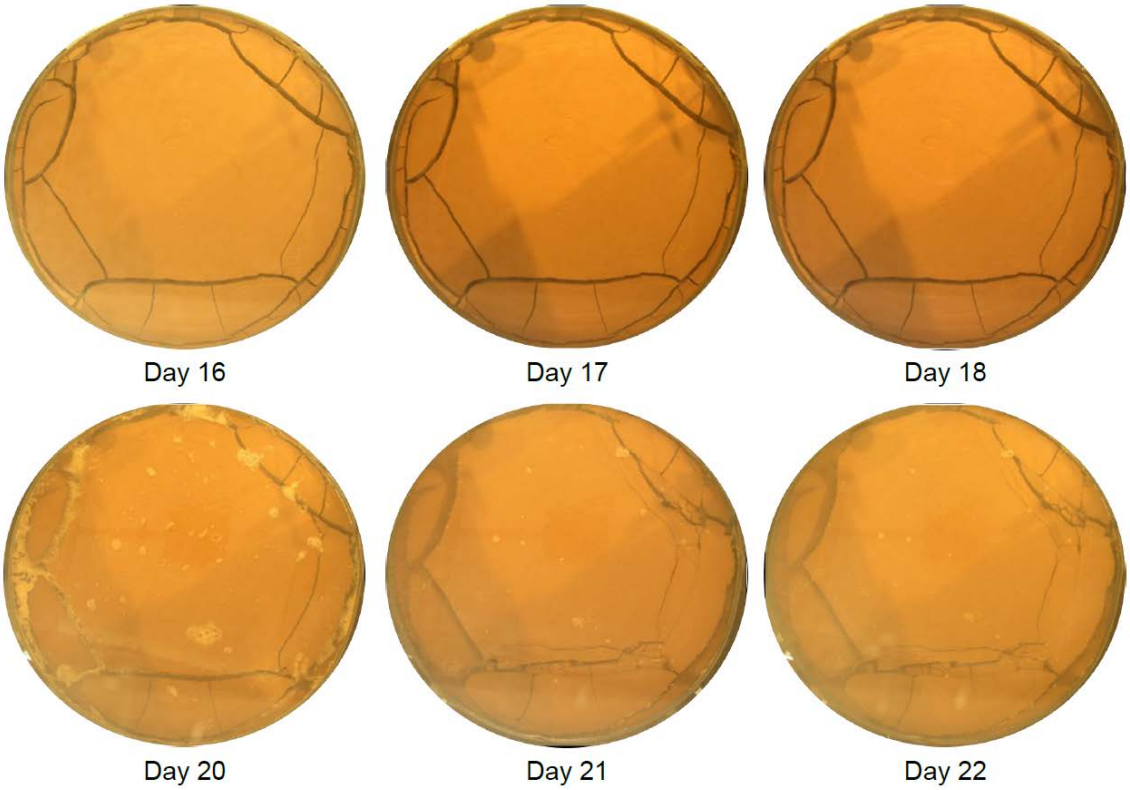

Figure 20 – Sequence showing the second and third stages: first wetting and flooding

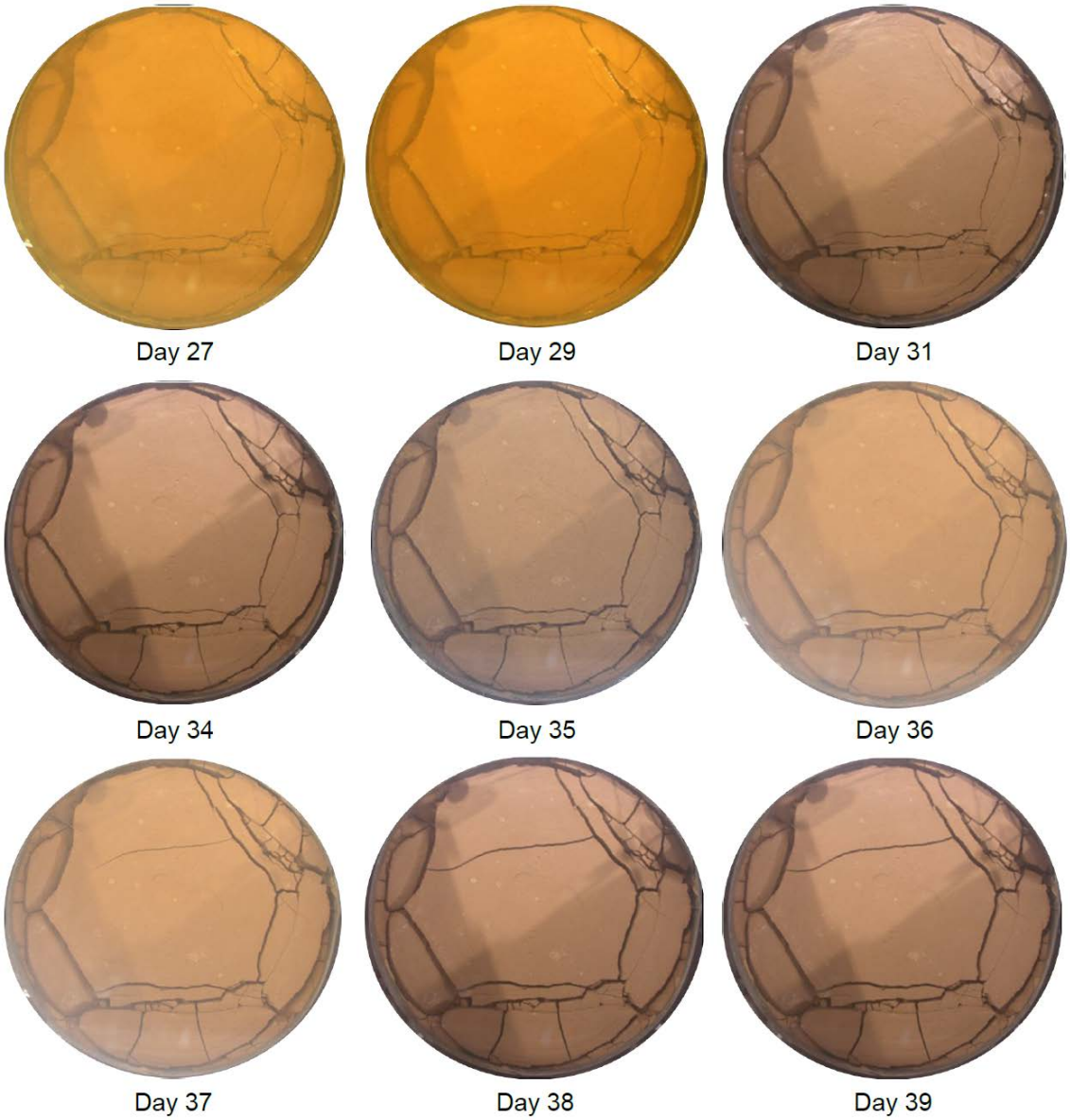

Figure 21 – Sequence showing the fourth stage: second drying

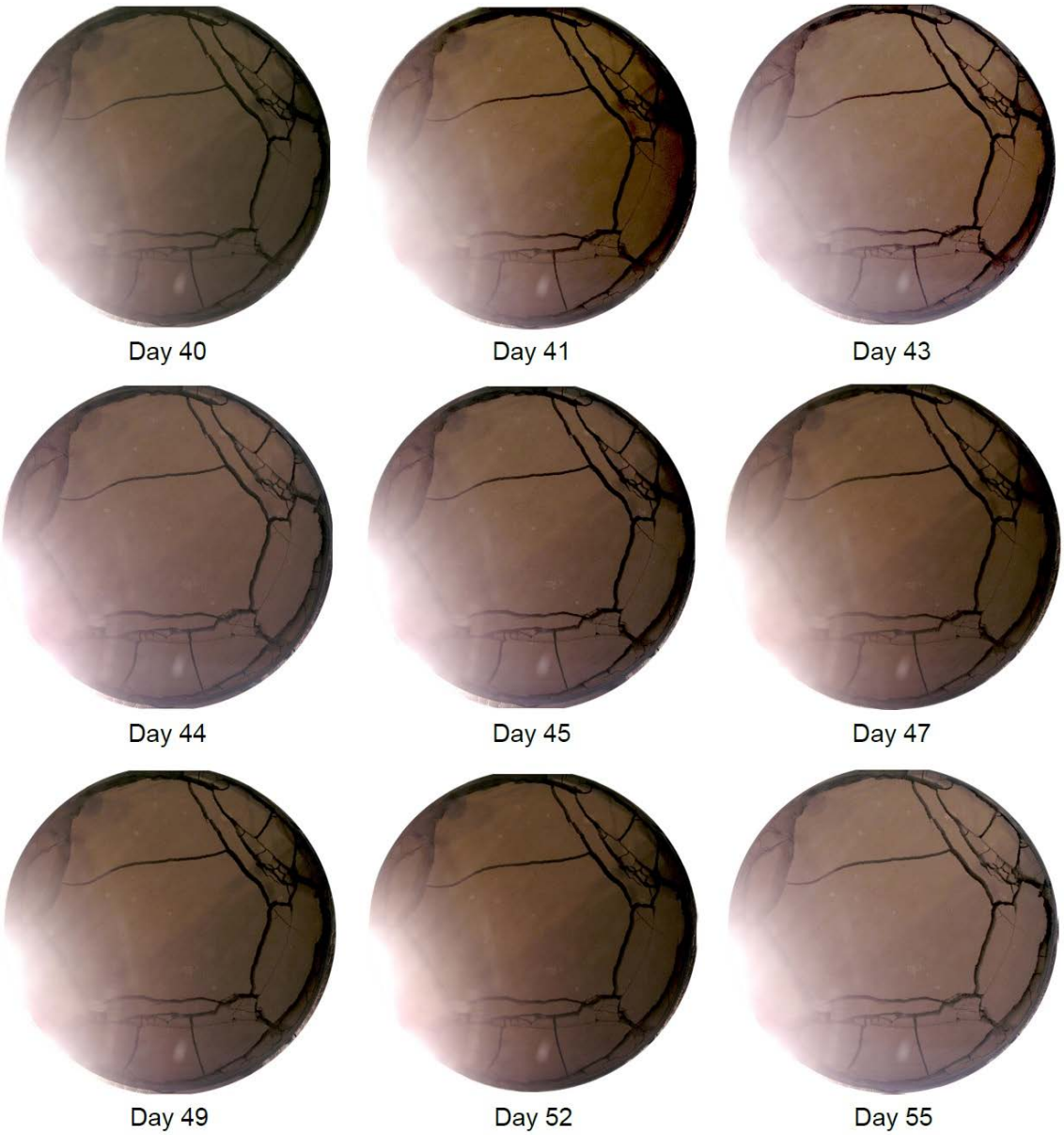

Figure 22 – Sequence showing the fifth stage: second wetting

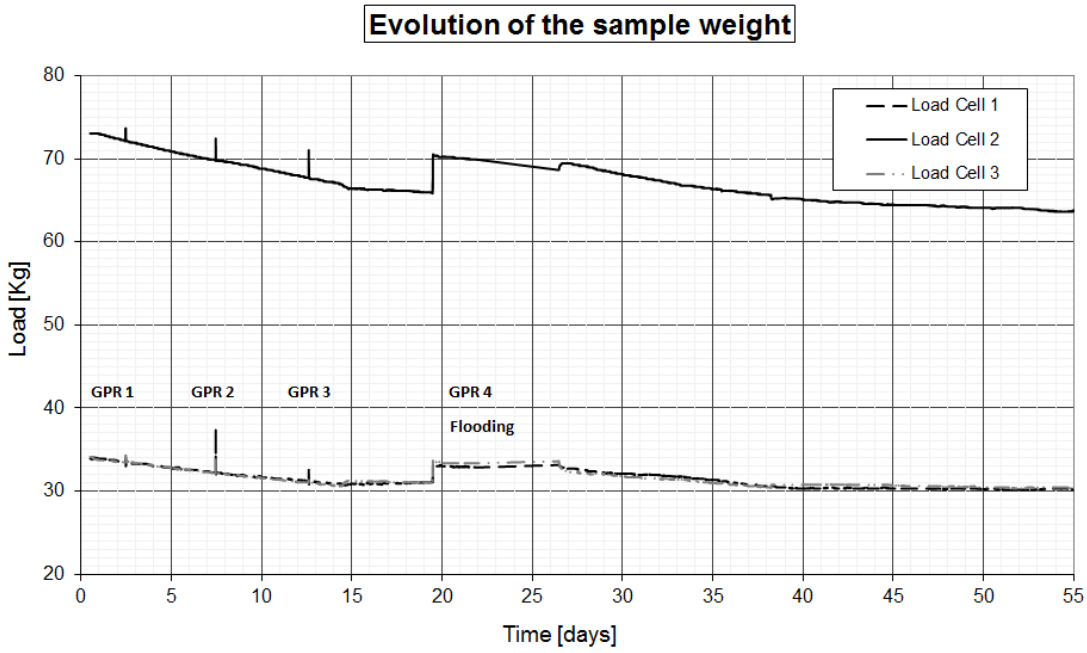

Figure 23 – Evolution of weight recorded with the load cells

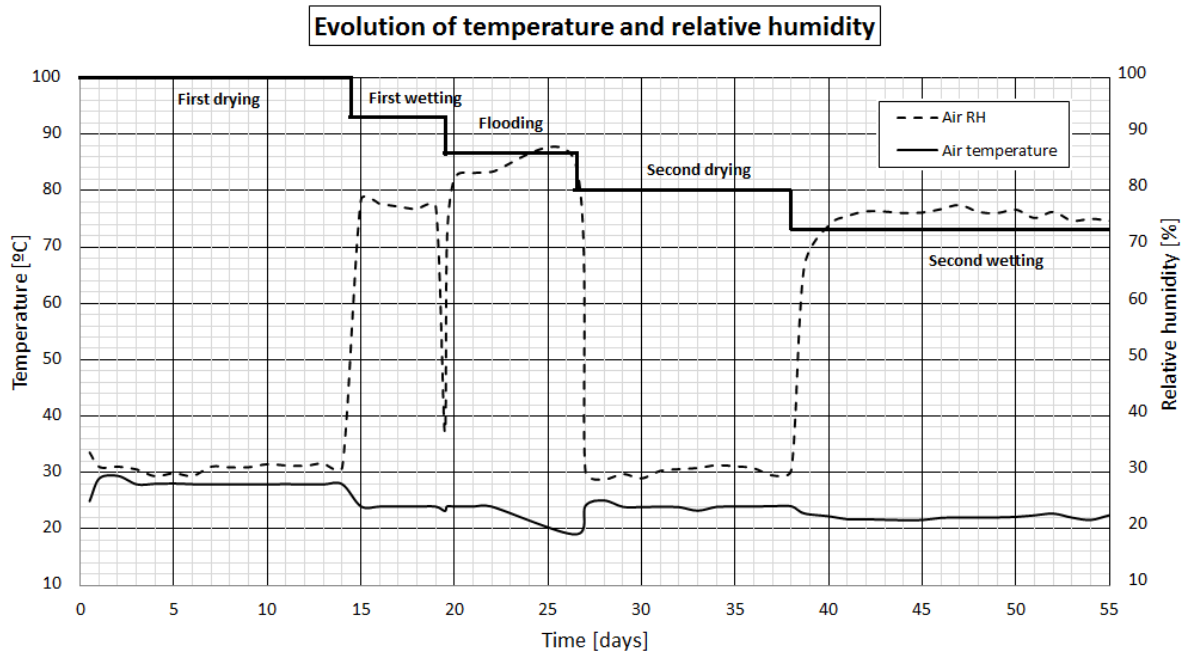

Figure 24 – Evolution of air temperature and relative humidity in the environmental chamber

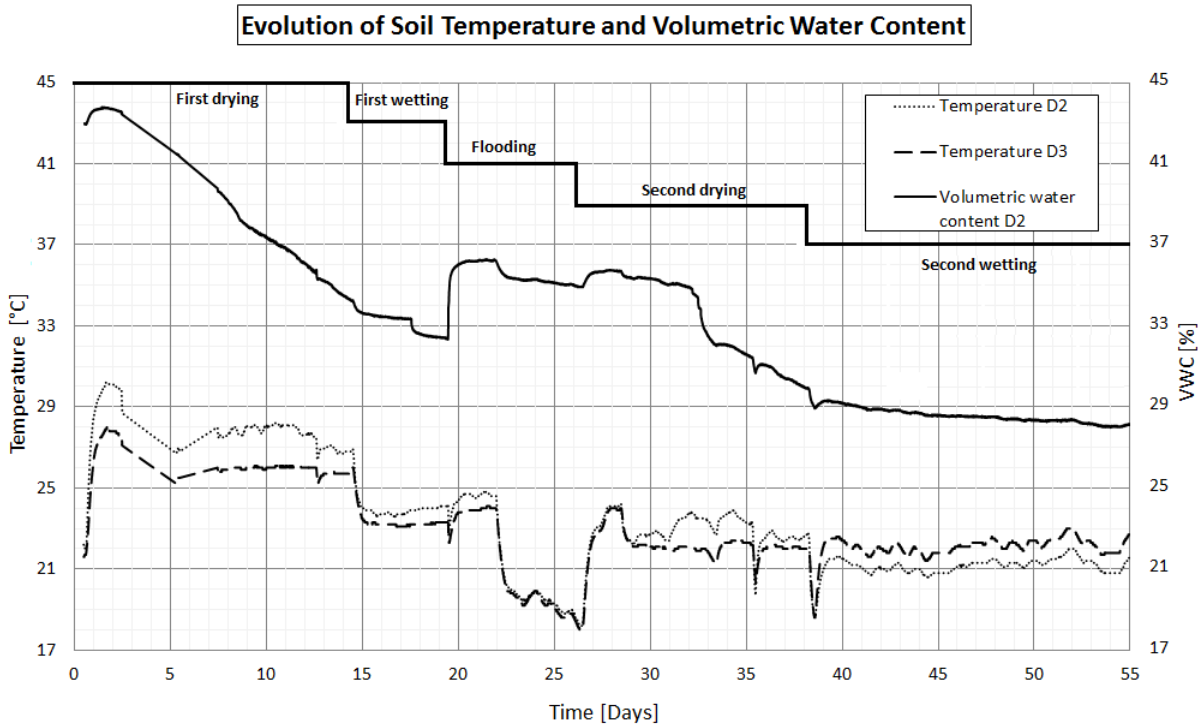

Figure 25 – Evolution of soil temperature and volumetric water content recorded with sensors 5TE (D2 and D3 in Figure 18)

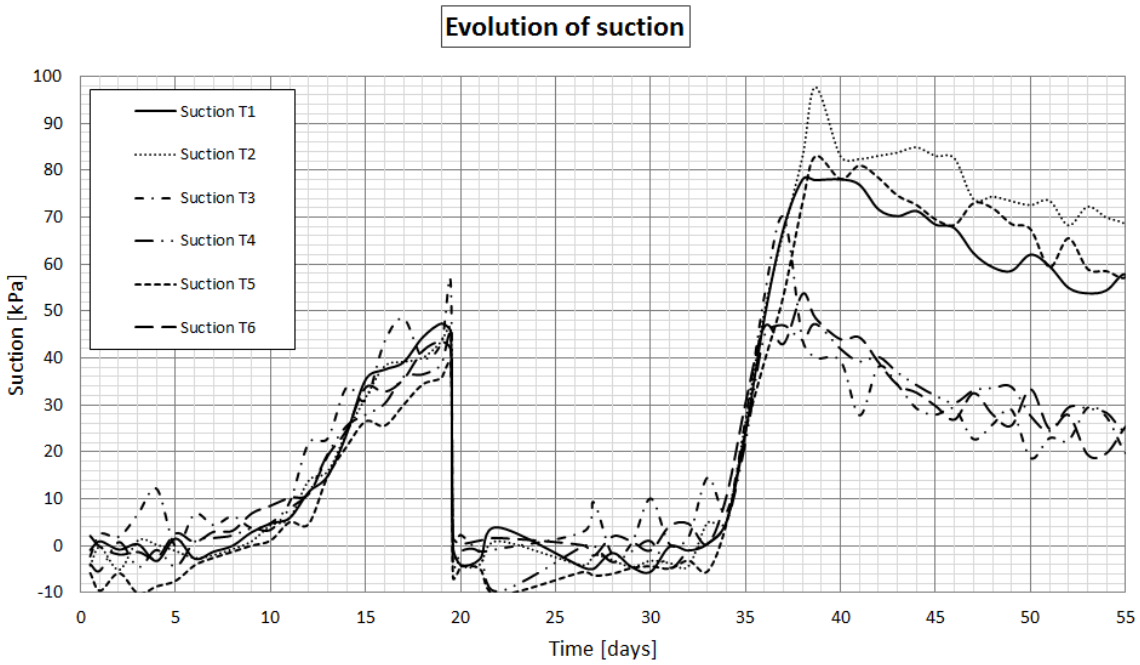

Figure 26 – Evolution of suction recorded with tensiometers T5X (T1-T6 in Figure 18)

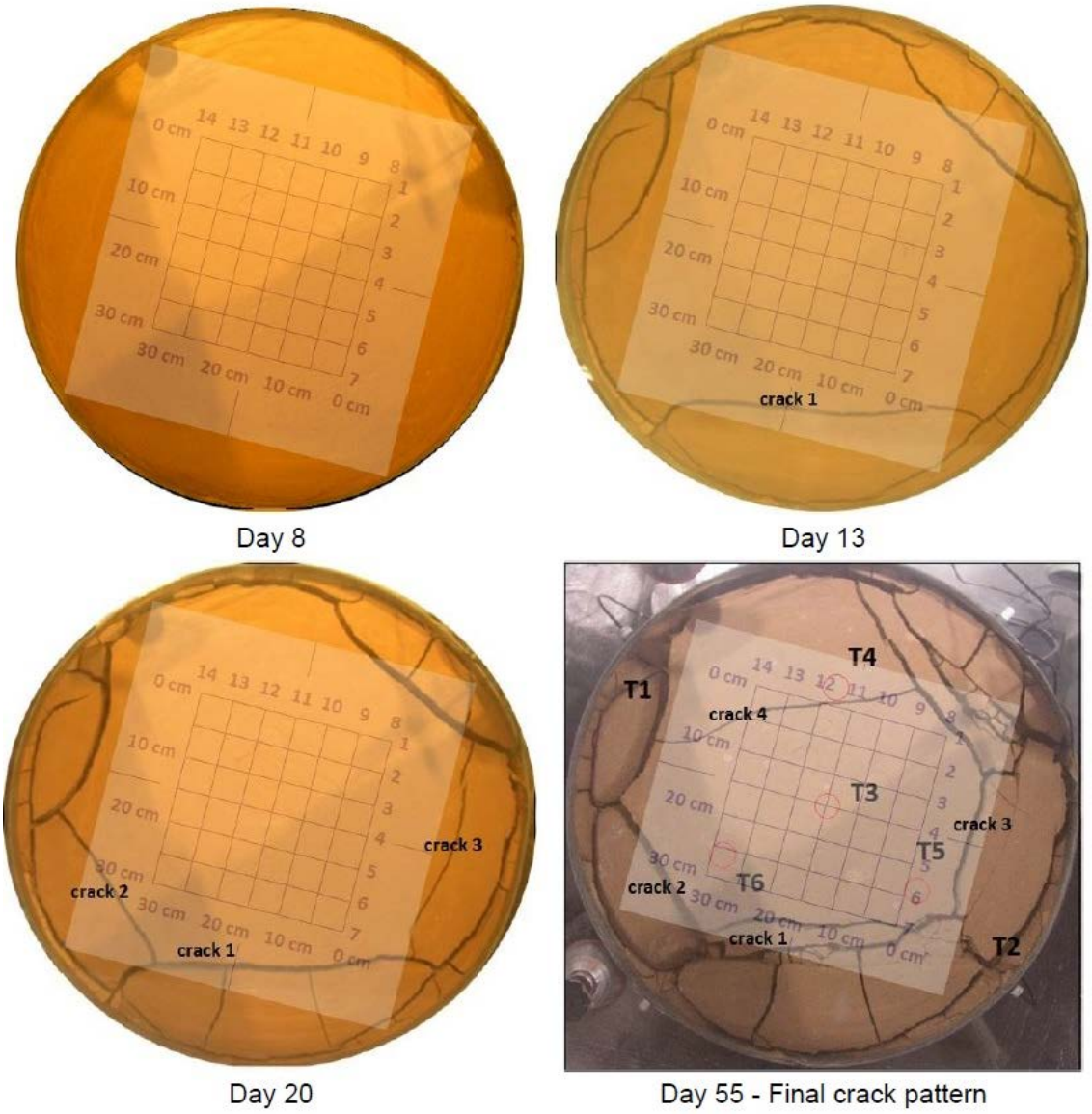

Figure 27 - Auscultation of the specimen with GPR during the cyclic test

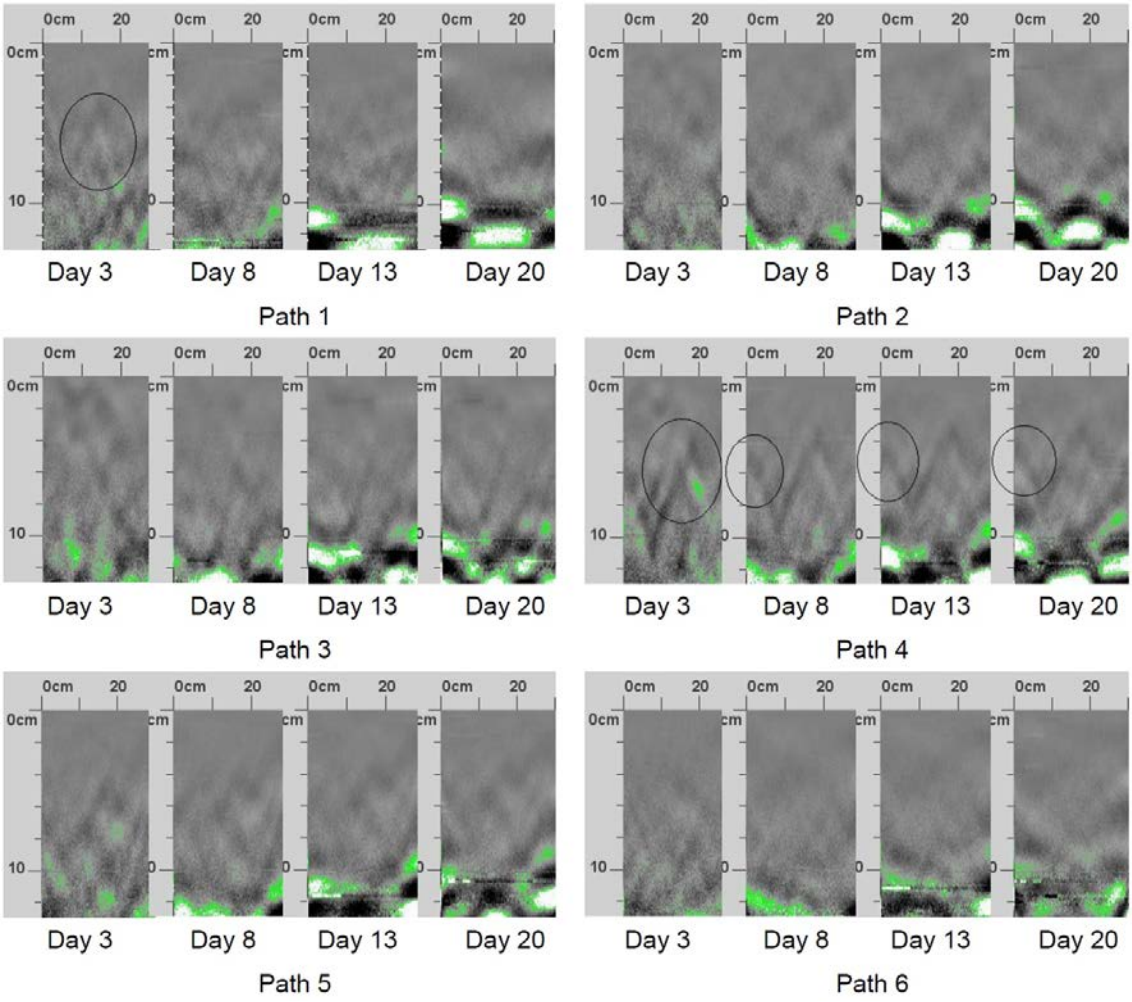

Figure 28 – Evolution of GPR profiles on paths 1-6 from day 3 to day 20

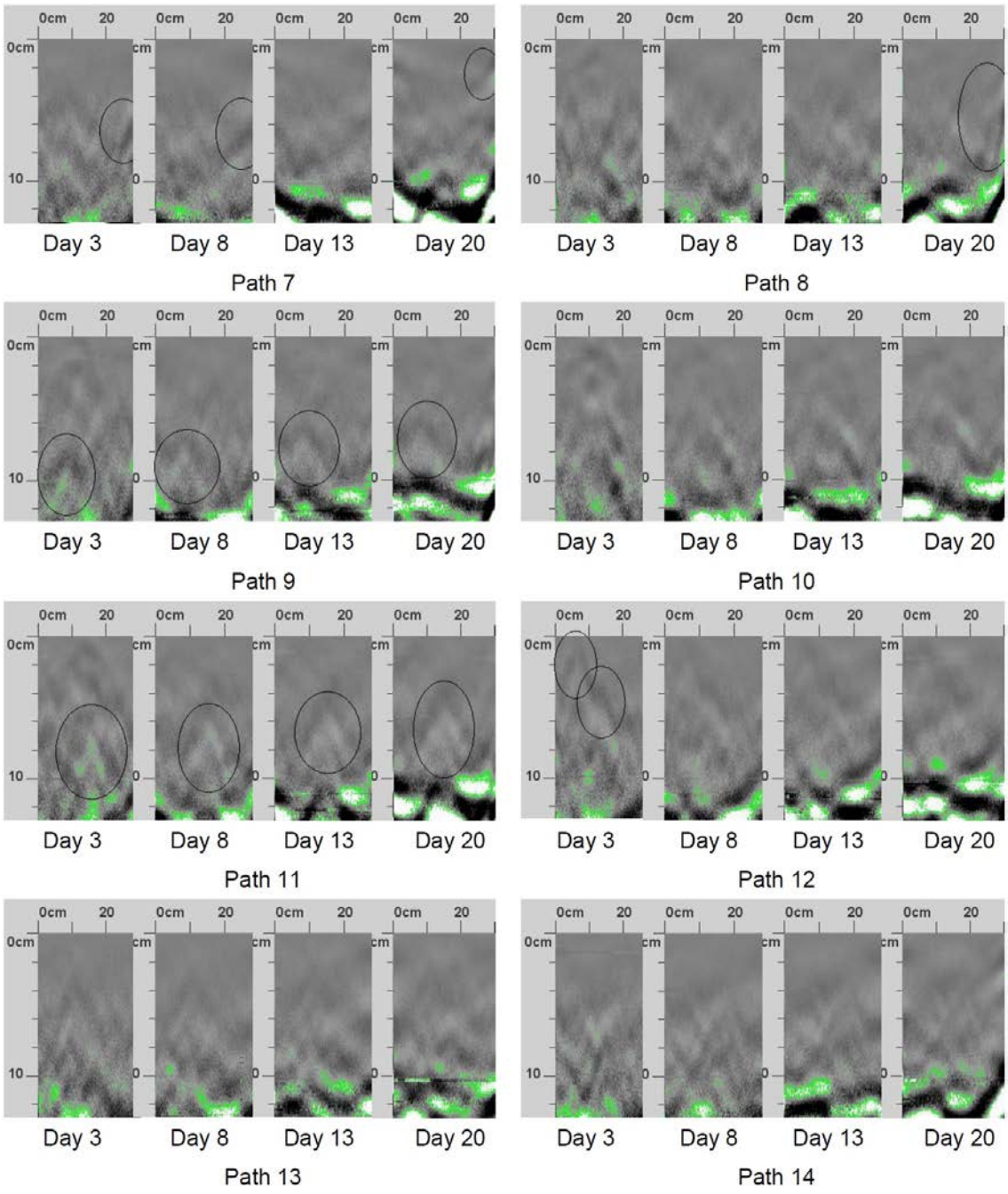

Figure 29 – Evolution of GPR profiles on paths 7-14 from day 3 to day 20